Low Temperature Plasma
Technology Laboratory

HELICON DISCHARGES AND SOURCES, A REVIEW

Francis F. Chen

LTP-1404 August, 2014

Electrical Engineering Department
Los Angeles, California 90095-1594

Helicon Discharges and Sources, a Review

Francis F. Chen, University of California, Los Angeles, 90095-1594

ABSTRACT

Helicon waves are waves in low-temperature, partially ionized plasmas in a dc magnetic field (B-field). The study of helicons involves both ion-neutral collisions and Larmor orbits, even when the B-field is uniform. Helicon discharges are ionized by helicon waves generated by a radiofrequency (RF) antenna. Interest in helicon discharges arose because of the high plasma densities they generate compared with other RF sources at comparable powers. The semiconductor industry has not taken advantage of this, even after the possible use of permanent magnets for the B-field had been demonstrated. Nonetheless, a large literature on helicons has evolved because of the numerous problems these discharges posed and the interesting physics found in their solutions.

I. A bit of history

In 1962 Peter Thonemann in the atomic energy laboratory at Harwell, UK, exclaimed, "Take a look at this: an electromagnetic wave at a low frequency!" Indeed, Lehane and Thonemann[1] had produced what they thought was a pure electromagnetic wave at about 15 MHz, much lower than known electromagnetic waves in plasmas…say, electron plasma waves in the GHz range or electron cyclotron waves, also in the GHz range at 500G (.05T). We now know that these "helicon" waves are largely electrostatic in spite of their excitation by an inductive antenna. The word HELICON is the name of a mountain in Greece and of a river in Scotland. "On the Banks of the Helicon" appears in the early music of Scotland. Here, helicon refers to the spiral nature of their waveforms and may have been chosen by Aigrain[2], who first studied these waves in semiconductors.

Among the early theorists were Leslie Woods[3,4], Legendy[5,6], Klozenberg et al.[7], Bleven et al.[8,9,10], Ferrari and Klozenberg[11], Davies and Christiansen[12] and Shoucri[13]. The Klozenberg paper gave the most complete treatment; but since it predated the invention of personal computers, the calculations gave meaningless results. Many a helicon neophyte has labored over this paper. One of the students in England was R.W. Boswell, who made helicons his major field of interest. Moving back to Australia and finishing his studies in 1970, he made a small helicon discharge with a new type of antenna (now called a Boswell antenna) which could be clamped onto a discharge tube without opening the vacuum[14]. At the Australian National University he established an active group working on helicons. In 1985, F.F. Chen visited his lab during his sabbatical from UCLA. He became interested in helicons and brought the idea back to T. Shoji[15] in Japan and to R.W. Conn in the U.S. Conn and student G. Campbell saw the possibilities and collaborated with Shoji to form the company PMT[16] to produce helicon sources for commercial use in semiconductor fabrication. An early application to plasma etching had been attempted by Chapman et al.[17] in 1991. The MØRI source of PMT was made into a successful array that passed "marathon" tests, but commercialization went no further. After the early work cited above, helicons have become an active field, and over 2700 papers have been published on them[18]. Major contributors have been[18] R.W. Boswell et al., E.E. Scime et al., S. Shinohara et al., F.F. Chen et al., and K. Shamrai et al. In addition, numerous researchers and groups in many countries throughout the world have joined in the effort to understand helicons.

Helicon waves have frequencies between the lower hybrid frequency $(\omega_c\Omega_c)^{1/2}$ and the ion plasma frequency Ω_p, and thus much lower than the electron cyclotron frequency ω_c. Initial studies therefore neglected the electron mass, though Boswell recognized that a second wave would exist when it was included[19]. This is now called the Trivelpiece-Gould (TG) mode. The first extensive papers describing helicons were published by Boswell[20] and by Chen[21,22]. The coupled helicon (H) and TG modes are described by four coupled first-order differential equations[23]. A computational program HELIC[24] for calculating the properties of H and TG waves, as well as for Inductively Coupled Plasmas (ICPs) with no B-field, has been written by D. Arnush[23].

In recent years the "double layer" created by a helicon discharge has attracted attention as a means of ion acceleration for spacecraft propulsion. C. Charles[25] has written a review of this field. The DC B-field required by helicon discharges is cumbersome for both industrial and propulsion applications. This constraint can be relieved by the use of permanent magnets[26,27]. Helicons are now widely known but have been put to practical use only in a few cases: for instance, in the fabrication of optical fibers[28] and in the propulsion of the Mars-bound spacecraft VASIMR[29].

II. Basic theory

Helicon waves are basically bounded whistler waves. Consider waves of the form $e^{i(m\theta+kz-\omega t)}$ propagating in a field $\mathbf{B} = B_0\hat{\mathbf{z}}$. The dispersion relation for electromagnetic electron cyclotron *R* waves at an angle θ to **B** is

$$\frac{c^2\beta^2}{\omega^2} = 1 - \frac{\omega_p^2/\omega^2}{1-(\omega_c/\omega)\cos\theta} \xrightarrow[\omega_c>>\omega]{} \frac{\omega_p^2}{\omega\omega_c\cos\theta}. \tag{1}$$

Here β is the total *k* such that $\beta^2 = k_\perp^2 + k_z^2$. Defining $k \equiv k_z = \beta\cos\theta$, we have

$$\beta = \frac{\omega}{k}\frac{\omega_p^2}{\omega_c c^2} = \frac{\omega}{k}\frac{n_0 e\mu_0}{B_0}. \tag{2}$$

This is the basic dispersion relation for helicon waves before we consider the complications. When the wave is confined to a cylinder of radius *a*, β is of order 1/*a*; and Eq. (2) shows how the parallel phase velocity varies with density and magnetic field.

In a long cylinder, the boundary condition for waves with $ka << 1$ is[30]

$$m\beta J_m(k_\perp a) = 0 \tag{3}$$

Most experiments generate the lowest radial mode with an $m = 1$ antenna, so that $k_\perp a$ is the Bessel root 3.83. Since $k_\perp \approx \beta$, Eq. (2) gives

$$\frac{3.83}{a} \approx \frac{\omega}{k}\frac{n_0 e\mu_0}{B_0} \propto \frac{\omega}{k}\frac{n_0}{B_0}. \tag{4}$$

This shows that, for a given mode, the density should be proportional to *B*. We shall find that this occurs at high B-fields, but at fields below about 0.01T there is a "low-field peak" which violates this general condition.

III. The TG mode

When the electron mass is kept finite, a second wave is excited along with the helicon wave. This is an electrostatic electron cyclotron wave[31] localized near the radial boundary. Propagating at an angle to a magnetic field, this wave has been named the Trivelpiece-Gould (TG) mode[32]. First found by Klozenberg[7] and by Boswell[33], the TG mode and its relation to the H mode has been treated theoretically by Shamrai and Taranov[34], Borg and Boswell[35], Chen and Arnush[36], and numerous other authors. Combining Maxwell's equations with the electron equation of motion, they obtained

$$\delta\nabla\times\nabla\times\mathbf{B}-k\nabla\times\mathbf{B}+k_w^2\mathbf{B}=0\,, \tag{5}$$

where $\delta = (\omega + i\nu)/\omega_c$, ν being the electron collision frequency with ions and neutrals, and

$$k_w^2=\omega n_0\mu_0 e/B_0\,. \tag{6}$$

Eq. (5) can be factored into

$$(\beta_1-\nabla\times)(\beta_2-\nabla\times)\mathbf{B}=0\,,\ \text{where} \tag{7}$$

β_1 and β_2 are the roots of

$$\delta\beta^2-k\beta+k_w^2=0\,. \tag{8}$$

These roots are, for $\delta k_w^2 << k^2$,

$$\beta_{1,2}=\frac{k}{2\delta}\left[1\mp\left(1-\frac{4\delta k_w^2}{k^2}\right)^{\frac{1}{2}}\right]\approx\frac{k}{2\delta}\left[1\mp\left(1-\frac{2\delta k_w^2}{k^2}\right)\right]\approx\begin{cases}k_w^2/k\\ k/\delta\end{cases} \tag{9}$$

The upper (−) sign gives the H mode, and the lower (+) sign the TG mode. An example of this relation between *k* and β is shown in Fig. 1. Eq. (6) shows that the curve depends on frequency, density, and B-field. The TG mode has large β and hence short radial wavelength. It is highly damped and therefore is localized near the boundary. The RF energy is often absorbed more by the TG mode than by the H mode. Figure 2A shows the undamped radial profiles of the H and TG modes; these are greatly altered by damping. Figure 2B shows the radial deposition profile computed with HELIC for a sample case. The small peak at $r = 0$ due to the H mode cannot be seen on this scale.

Presence of the TG mode has been seen in experiment[37]. It can be shown[37] that TG mode affects the current profile $J(r)$ more than the field profile $B(r)$, and amplitude peaks at the edge due to the TG mode can be seen in Fig. 3.

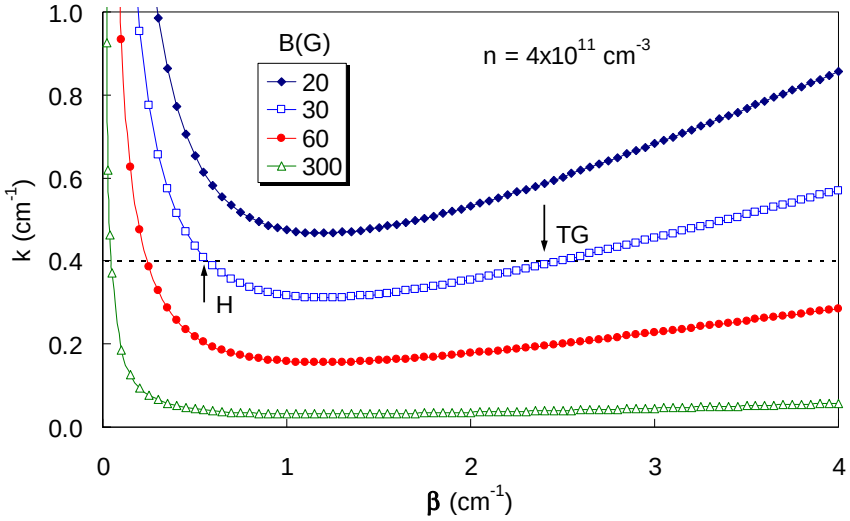

Fig. 1. Example of the $k - \beta$ relation for coupled $m = +1$ helicon and TG waves at 11 MHz in a tube of 2.5 cm radius (Ref. 36).

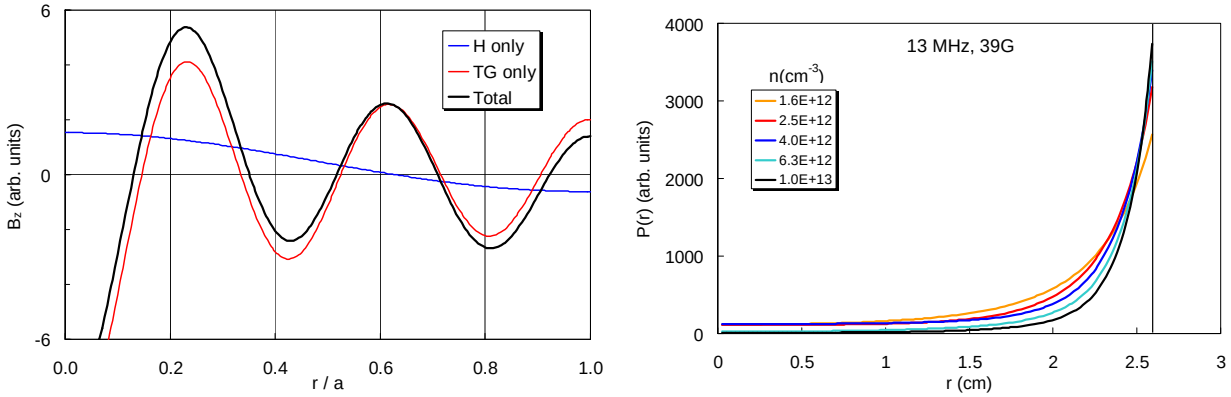

(A) (B)

Fig. 2. (A) Example of undamped $B_z(r)$ showing the H and TG modes separately (10^{12} cm^{-3}, 30G, $m = 0$). (B) Example of an RF radial energy deposition profile showing the dominance of the TG mode.

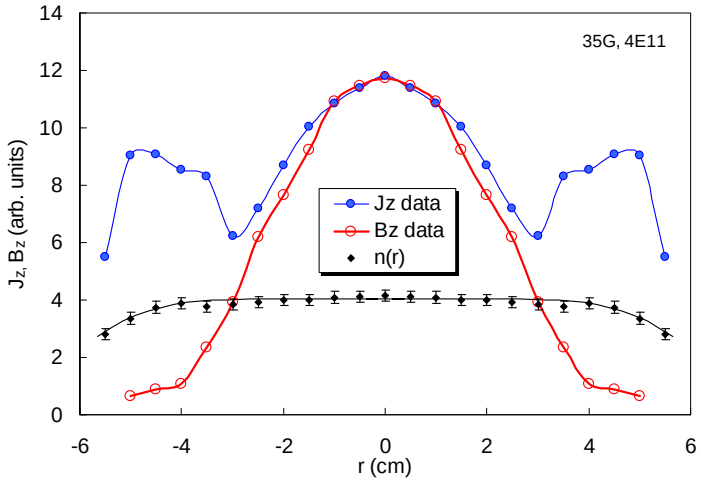

Fig. 3. Profiles of $|B_z|$ (•), $|J_z|$ (o), and density measured in a helicon discharge 6 cm in radius and 110 cm long, with 1 kW of 11 MHz RF power at 2 mTorr of argon (Ref. 36).

IV. Mode patterns

The electric field patterns for azimuthal wave numbers $m = \pm 1$ are shown in Figs. 4 and 5[21]. The $m = -1$ mode has a much narrower profile, which may be the cause of its weaker propagation, as we shall see. The mode pattern for the $m = 0$ mode in Fig. 6 is entirely different: the wave changes from pure electrostatic to pure electromagnetic in each half-cycle.

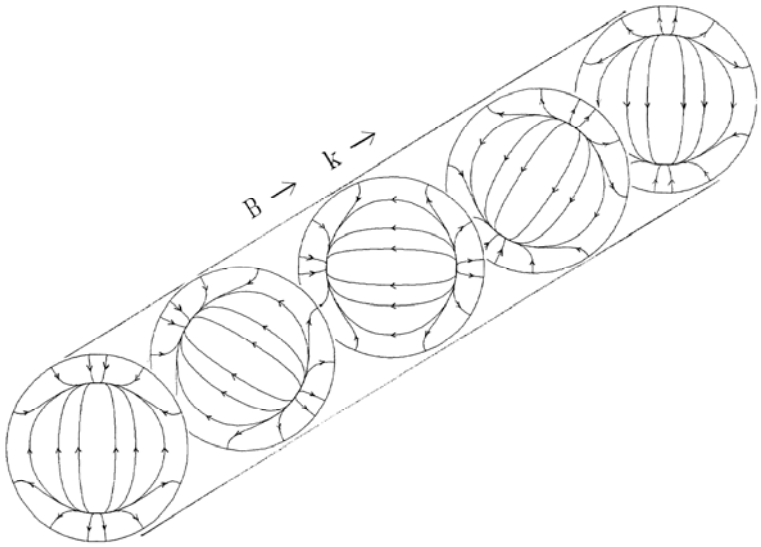

Fig. 4. The $m = +1$ mode pattern rotates clockwise as seen by a stationary observer.

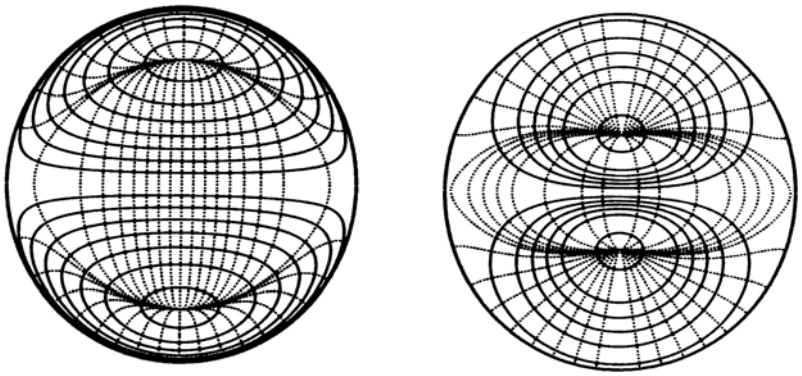

Fig. 5. E-field patterns of the $m = +1$ (left) and $m = -1$ (right) modes.

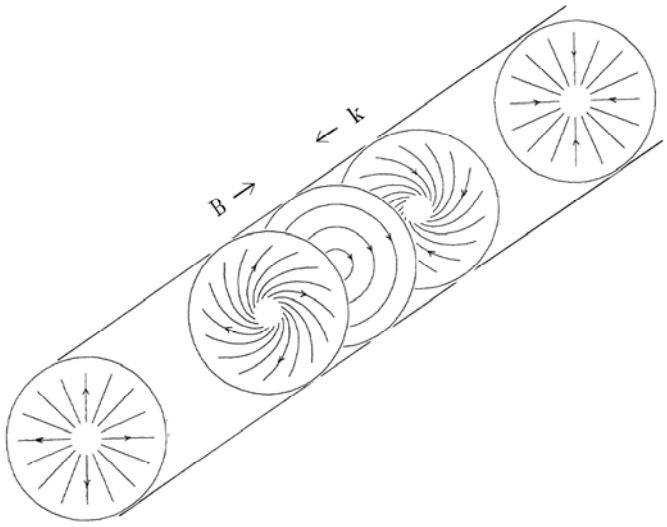

Fig. 6. Mode patterns of the $m = 0$ helicon mode.

V. Antennas

In experiments on rf plugging of mirror machines, Watari *et al*.[38] found that one type of antenna excited much larger RF fields in the plasma than the others. The reason for this was not known until the antenna was used in the Dawson Separation Process for purifying uranium using ion cyclotron waves. John Dawson's explanation, repeated here, had been published only in a book celebrating his 60th birthday[39]. Figure 7 shows a full-wavelength Nagoya Type III antenna. Normally only half of this is used and is sufficient.

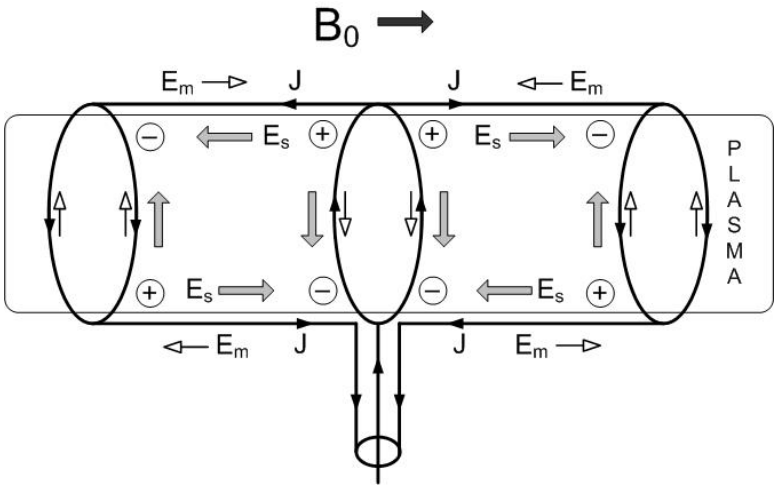

Fig. 7. Diagram of a Nagoya Type III antenna.

In a rising half-cycle, the rf current enters from the cable, splits in half at the center ring, and goes around the plasma to reach the top horizontal leg. There it splits again and goes left and right to the two end rings, where the current again goes around the plasma to reach ground via the bottom horizontal leg. Consider the top leg. As the current **J** rises, it generates a field $\mathbf{E_m}$ which opposes the rise. That field pushes electrons away from the center ring. Electrons then pile up near the end rings, leaving a positive space charge near the center ring. These charges generate an electrostatic field $\mathbf{E_s}$ pointing away from center. The field $\mathbf{E_s}$ builds up until it stops the electron flow along $\mathbf{B_0}$. At the same time, the opposite currents and charges are created near

the bottom leg. The antenna thus creates a pattern of space charges marked ⊕ and ○ on the diagram. These space charges in turn create a transverse E-field perpendicular to $\mathbf{B_0}$, as indicated by the heavy arrows. This vertical E-field is in the same direction as the $\mathbf{E_m}$ field of the ring currents but is much stronger, since the space charges were collected over the length of the antenna. The longer the antenna, the larger the space charge must be to cancel the field $\mathbf{E_m}$. Hence, the antenna amplifies the applied rf field by creating electrostatic fields. It can be shown[40] with a rectilinear model of the antenna that the amplification factor is approximately $(k_\perp^2/k_\parallel^2)$, where the k's are the antenna wavenumbers perpendicular and parallel to $\mathbf{B_0}$.

The Boswell antenna, shown in Fig. 8, is a modified Nagoya antenna with the top and bottom legs split into two wires so that the antenna consists of two separate halves. The advantage of this is that the antenna can be slipped around a cylindrical discharge tube without breaking the vacuum.

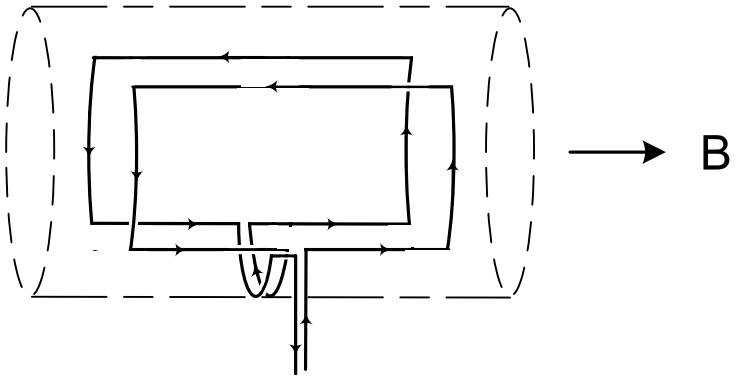

Fig. 8. Schematic of a Boswell antenna.

As shown by Miljak[41], helical antennas are Nagoya antennas twisted into right- or left-handed helices to better match the fields of the helicon wave. A "right-helical" antenna, with azimuthal mode number $m = +1$, is shown in Fig. 9. This antenna creates much higher plasma densities than the left-helical $m = -1$ antenna, which is comparatively ineffective. The reason is not entirely clear, although the field patterns of the two are somewhat different (Fig. 5). The Nagoya antenna, being symmetric, generates both $m = +1$ and $m = -1$ fields, but the discharge is almost entirely due to the $m = +1$ mode.

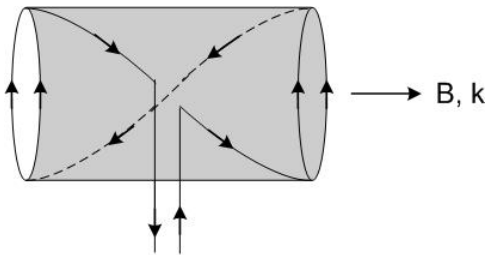

Fig. 9. Schematic of a half-wavelength right-helical antenna.

In the $m = \pm 1$ case, the same field pattern simply rotates as seen by a stationary observer (Fig. 4). The presence of electrostatic space charges can be seen from the convergence and divergence of the field lines at an intermediate radius. The azimuthally symmetric $m = 0$ helicon mode has an entirely different nature, as seen in Fig. 6. The E-field lines change from solenoidal (electromagnetic) to radial (electrostatic) in every half cycle, with a mixture in between. Thus, the RF E-field there and the RF B-field are of equal importance. Such $m = 0$ antennas have been used commercially either singly or in pairs with currents in the same or opposite directions.

Matching the 50-Ω output of RF power supplies to the inductance of the antenna (the resistance of the plasma is small) is usually done with variable vacuum capacitors. The initial setting of these capacitors has to be close enough to ignite the discharge, after which the capacitors can be set to minimize the reflected power, done either manually or with an automatic tuning network. For given values of the antenna inductance and plasma resistance, the starting values of the capacitances can be found algebraically[42].

VI. Landau damping

The phase velocities of helicon waves, as predicted by Eq. (4), can be comparable with electron thermal velocities, thus raising the possibility that electrons "surfing" on these waves can be accelerated to ionizing energies, thus causing the helicons' high RF absorption efficiency[21]. This proposed mechanism was adopted by numerous authors[43,44] and was supported by detection of fast electrons by Ellingboe et al.[45] using RF-modulated emission of Ar^+ light. However, Molvik et al.[46] and Chen and Blackwell[47] showed with gridded energy analyzers that the number of fast electrons was insufficient to provide all the ionization in a helicon discharge. It was the TG mode described above that was the main ionization mechanism. Thus, the connection of helicons with Landau damping has turned out to be unimportant.

VII. The HELIC code

After the invention of personal computers, numerous theorists have devised codes for calculating helicon properties[48,49,50,51]. There have been many others, but the only code that has a user interface and is open-source[52] is the HELIC program by D. Arnush[23], which solves the following coupled first-order differential equations:

$$\begin{aligned}
&\frac{\partial E_\varphi}{\partial r} = \frac{im}{r}E_r - \frac{E_\varphi}{r} + i\omega B_z \\
&\frac{\partial E_z}{\partial r} = ikE_r - i\omega B_\varphi \\
&i\frac{\partial B_\varphi}{\partial r} = \frac{m}{r}\frac{k}{\omega}E_\varphi - \frac{iB_\varphi}{r} + \left(P - \frac{m^2}{k_0^2 r^2}\right)\frac{\omega}{c^2}E_z \\
&i\frac{\partial B_z}{\partial r} = -\frac{\omega}{c^2}iDE_r + \left(k^2 - k_0^2 S\right)\frac{E_\varphi}{\omega} + \frac{m}{r}\frac{k}{\omega}E_z
\end{aligned} \tag{10}$$

These equations follow from Maxwell's equations and the cold-plasma equations with the familiar S, P, D dielectric elements[53]. They are derived in three papers by Arnush[23,36,54]. HELIC solves these equations for each k of the antenna spectrum, and for each value of n and B_0. A typical run for $R(n,B)$, as in Fig. 14 below, takes about $1-2$ hours on a personal computer. Figure 10 shows the geometry used for the HELIC code. The antenna can be any of the common types and can be located at any distance from one endplate. The endplate separation can be specified. The assumed plasma can vary radially but not axially. For short discharges, the assumed radial profile can be calculated from a recent theory[50].

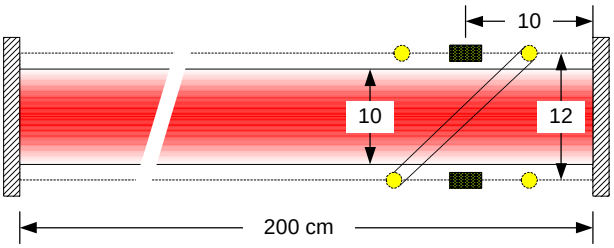

Fig. 10. Geometry of the HELIC code. Here the assumed diameters of the plasma and the antenna, and the antenna position are given in cm.

Figure 11 shows the input and output pages of HELIC desktop. The inputs include 1) the discharge and antenna radii, the discharge gas and frequency, the antenna type and distance from an endplate; 2) the ranges of density and B-field to be calculated, either linearly or logarithmically spaced; the radial density, temperature, and pressure profiles; and 3) some calculational choices. The outputs include the power spectrum of the antenna, the radial and axial deposition profiles, all the wave fields vs. r and z, and, most importantly, R(nB), which is the plasma resistance vs. n and B_0. This quantity should be $\geq 1\Omega$ for the RF power to be deposited mostly in the plasma rather than in the circuitry. The wave fields can be obtained with the H and TG parts separated. At high B-fields, these modes merge and cannot easily be identified. A high-field formulation of the equations has then to be used, and Arnush has provided an adjustable point for transition to the high-field case.

Figure 12 is an example of a plot of $P(r)$, the radial power deposition profile. Note the transition from H-mode to TG-mode deposition as the density is increased. Figure 13 is an example of the axial power profile $P(z)$. We see that much of the power is deposited downstream of the antenna. There is also a small peak at the endplate, where the wave is reflected. Figure 14 is a plot of $R(n)$ for various B_0 showing peaks in R. These are the low-field peaks to be discussed later. The plasma losses are proportional to n and can be represented by a straight line. The operation point is the intersection of this line with the right-hand side of one of the curves. This is the stable point[55], since the loading increases with a decrease in n, and *vice versa*. Such curves are used only as guides for the design of an experiment.

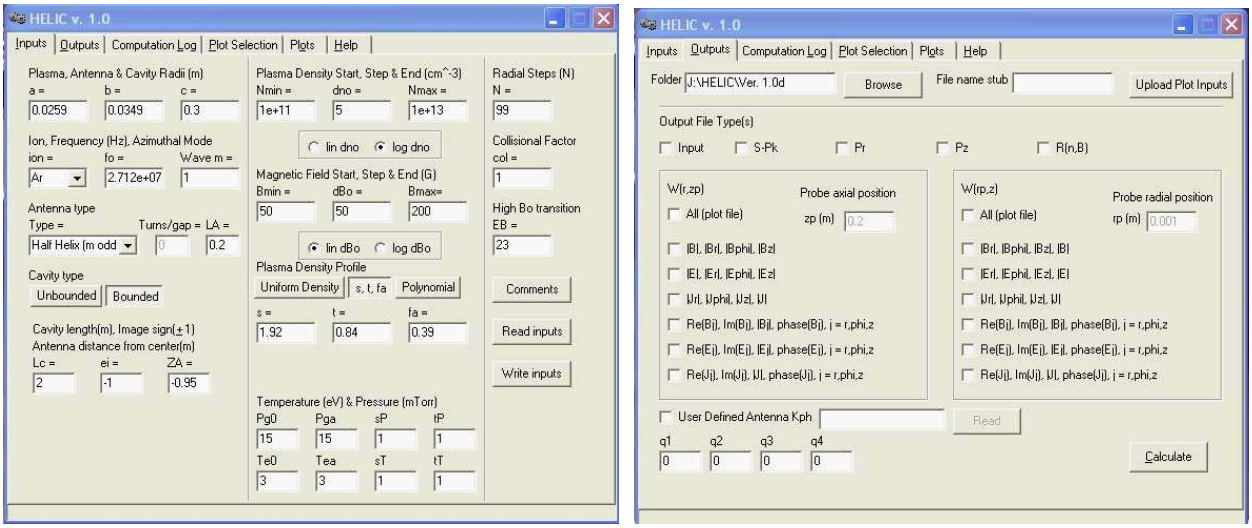

Fig. 11. The input page (left) and output page (right) of the HELIC program.

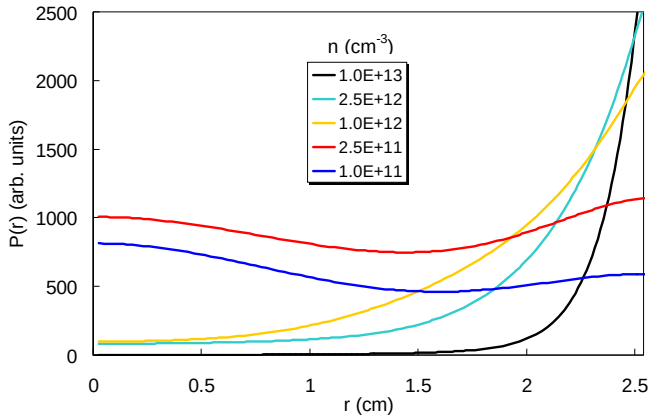

Fig. 12. Example of a HELIC calculation for radial power deposition profile in a single-ended cylinder of 2.5 cm radius. The 50G (.005T) discharge is at 27.12 MHz in 15 mTorr of argon. The $m = 0$ antenna of 3.49 cm radius is 5 cm from the endplate. KT_e is assumed uniform at 3 eV, but the density has a "universal" profile (Ref. 50). The legend refers to the curves from top to bottom at the extreme right.

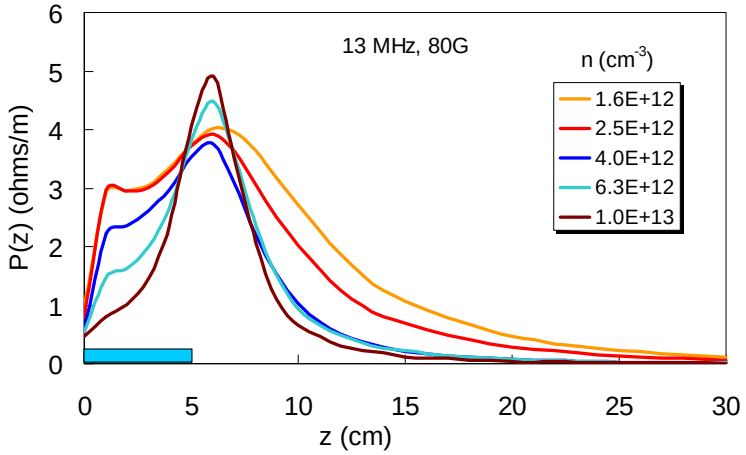

Fig. 13. Example of a HELIC calculation of axial power deposition profile in the tube specified in Fig. 11, but at 13.56 MHz and 80G (.008T). The legend lists the curves in the order of peak height (not uniform). The location of the tube is shown at the bottom.

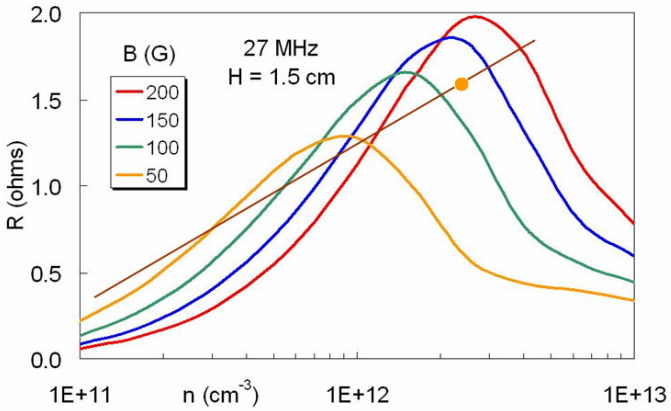

Fig. 14. Example of $R(n,B)$ curves calculated by HELIC for a 5.1-cm diam tube with an $m = 0$ antenna 1.5 cm from the endplate. The energy losses are represented by the straight line. The dot shows an operating point at $n \approx 10^{12}$ cm^{-3}.

The HELIC code made it possible to design the diameters and lengths of helicon discharges for operation at various magnetic fields and densities, as long as n, B, and T_e are uniform in the direction of **B**. Similar curves have been obtained by Suwon Cho et al.[56,57,58,59].

VIII. The low-field peak

In early experiments on helicons[60], it was observed that when the field lines terminated on the glass tube, as shown in Fig. 15, the discharge was effectively bounded by an insulating endplate. The density was then increased over the case of a uniform field (Fig. 16). In the same device, it was found that n did not increase monotonically with B_0, as predicted by Eq. (2) but had a small peak (Fig. 17) at low fields of the order of 60G (.006T). This low-field peak[61,62] could also be produced with a conducting endplate, also shown in Fig. 18. In either case, the explanation is that the helicon wave is reflected constructively from the end boundary (with opposite phase for conductors and insulators), thus increasing the ionization and the density. This mechanism is illustrated in Fig. 18. To confirm this, HELIC computations were made for unidirectional and bidirectional antennas, as shown in Fig. 19. The peak occurs strongly for simple loop antennas, which are bidirectional. The low-field peak has also been seen by Sato et al.[63] and explained by S. Cho[64]. This effect will be used in compact permanent-magnet helicon sources described later.

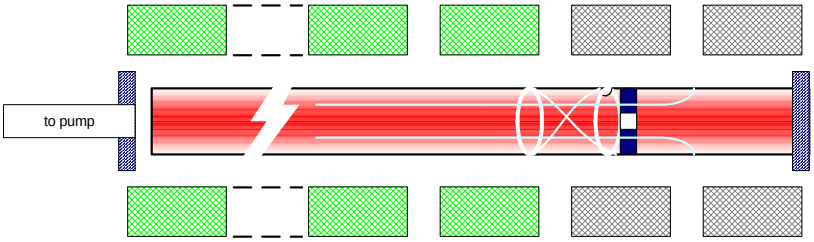

Fig. 15. A helicon discharge ending on an insulator or a conducting endplate (not at the same time). The cusped field is formed by turning off the two end coils. (Ref. 54).

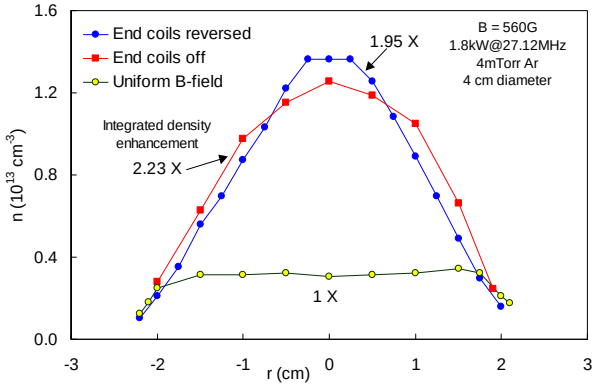

Fig. 16. Density enhancement with magnetic cusps at the ends of the discharge (Ref. 70).

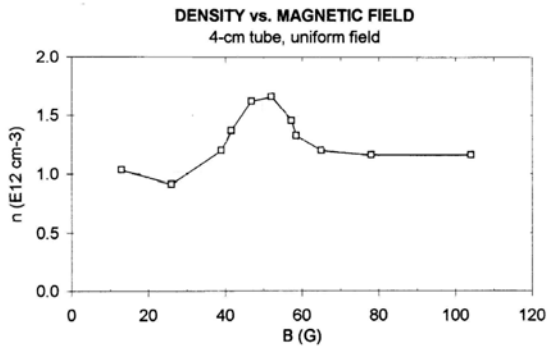

Fig. 17. A low-field density peak (Ref. 60).

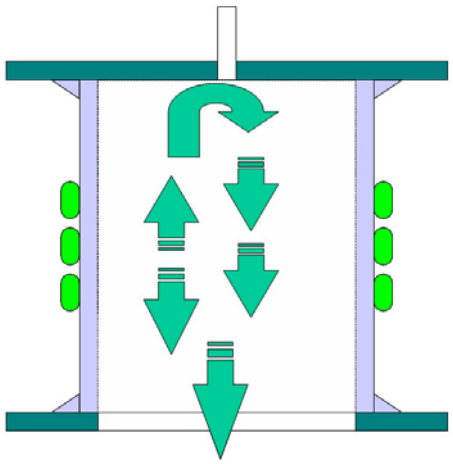

Fig. 18. Mechanism of the low-field peak.

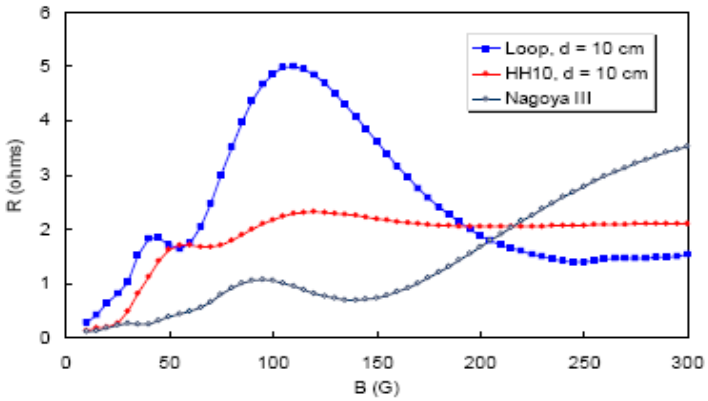

Fig. 19. HELIC calculations of $R(B_0)$ for bidirectional and unidirectional (HH10, helical) antennas.

IX. Early experiments

This review of experiments does not differentiate between pulsed and steady-state discharges. To limit the heating of probes and O-rings, the RF is often pulsed for 10-1000 msec, during which the plasma reaches equilibrium and measurements can be made. In steady-state operation, the neutral density can reach its equilibrium profile also. Fast probes have been made in the past to sample dense DC discharges.

The first large helicon discharge was built by Boswell in Australia. The BASIL machine[65], 4.5 cm in diameter and 160 cm long, had B_0 up to 1600 G (0.16T), RF power (P_{rf}) up to 5 kW at 7 MHz. Running at 1 Pa of argon, it achieved a peak density of 10^{20} m^{-3}. A second machine, the WOMBAT[20], shown in Fig. 20, had a helicon source 18 cm in diameter and 50 cm long, injecting the plasma into a large chamber 90 cm in diameter and 200 m long. As power or B-field is increased, a radiofrequency discharge changes from a capacitive to an inductive to a helicon discharge, as shown by Degeling *et al*.[66]. The transition into a helicon discharge as the RF power was increased was shown by Chi *et al*.[67] and by Ellingboe *et al*.[68] As seen in Fig. 21a, the RF at low power is capacitively coupled to the plasma via the voltage on the antenna. A higher power it is the RF magnetic field which excites currents in the plasma after the gas breaks down from the E-field. Finally, the power is high enough to generate a density matching the helicon conditions. Jumps can also be seen at constant B-field and increasing power, as seen in Fig. 21b[20]; in this case, the jumps are from one helicon mode to another. An alternative explanation of jumps was later suggested by Chen and Torreblanca[69]. A jump can occur when the plasma resistance R exceeds the circuit resistance. This was verified in their experiment.

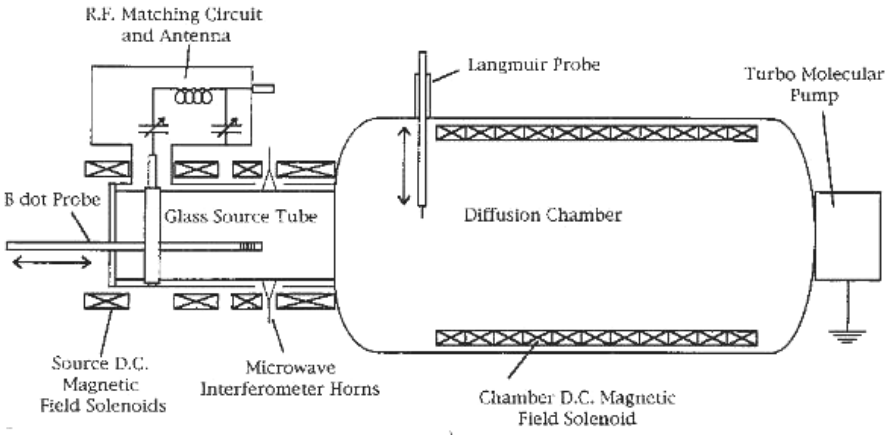

Fig. 20. The Australian WOMBAT machine (Ref. 20).

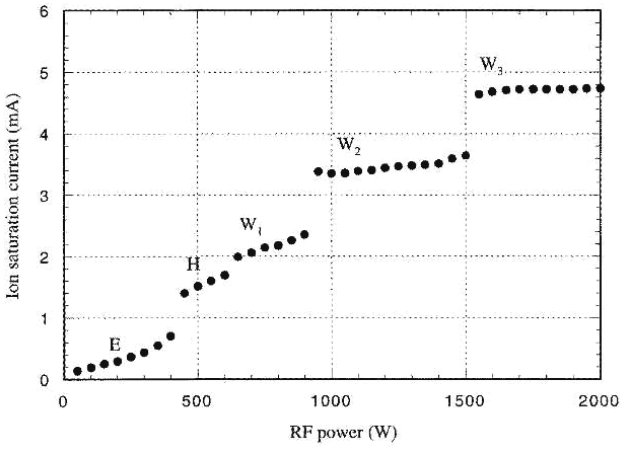

Fig. 21a. Density jumps vs. RF power (Ref. 67).

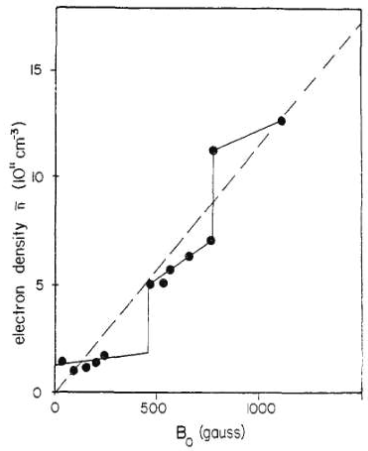

Fig. 21b. Mode jumps vs. B_0 (Ref. 19).

After bringing the helicon idea to the U. S., Chen built the linear experiment shown in Fig. 22. The coils were mounted as received from the factory without rewinding, leaving gaps for probes. The original matching circuit used waveguides with sliding stubs; vacuum capacitor units were available later. The coils and the RF were pulsed for <100 msec, thus avoiding water

cooling. These early experiments[70] tested the Nagoya and helical antennas and the effect of cusp fields at the endplate. The antenna studies by Miljak[41] were also done on this machine.

A larger machine (not shown), with a 10-cm diameter tube 108 cm long, with pulsed fields up to 0.1T, was built by D. D. Blackwell[71]. Figure 23 shows end views of the discharge in 488 nm Ar^+ light. In 23(A), the discharge is just above the jump from capacitive to inductive coupling and shows the location of the antenna bars at top and bottom. After addition of a Faraday shield in (B), the discharge is more symmetric with the removal of the antenna's E-field. In (C), a helical antenna produces a dense, symmetric plasma. This is seen as a narrow, bright blue column, even in smaller 5-cm diameter discharges, and has been named the Big Blue Mode. We surmise that it occurs because of an ionization instability: as neutrals are depleted, electrons make fewer collisions, and KT_e rises. This increases the ionization rate exponentially. The asymmetry seen in (C) is caused by a Langmuir probe.

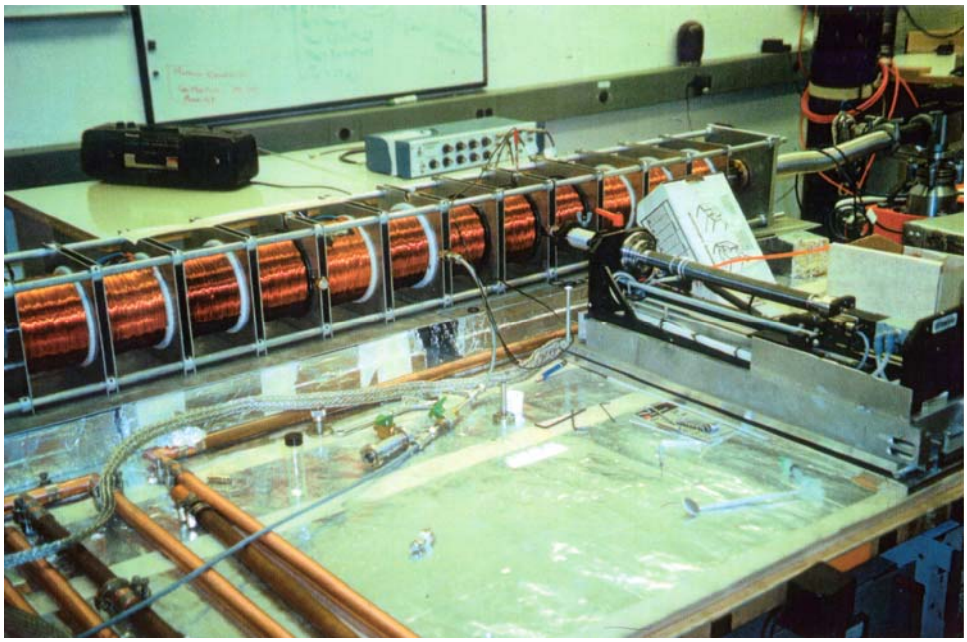

Fig. 22. The first helicon experiment in the U.S.

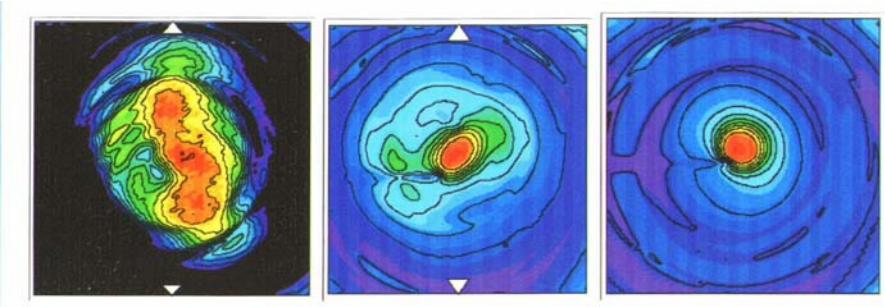

A B C

Fig. 23. End views of a helicon discharge with A) a straight Nagoya III antenna with no Faraday shield, B) the same antenna with a Faraday shield, and C) a right-helical antenna with or without shield (Ref. 71).

A side view of this discharge in Fig. 24, taken at three ports, shows the difference between $m = +1$ and $m = -1$ helical antennas. Though the light intensity differences are not clear in these early data, the $m = -1$ antenna generates a low-density plasma that fades axially. The *m*

= +1 antenna gives a long, dense plasma. The straight, bidirectional Nagoya antenna gives a less dense plasma that also reaches the end of the tube.

An experimental check of theory for radial B_z profiles was performed by M. Light[72] using a loop probe. Shown in Fig. 25 are measured and computed profiles for the case $\mathbf{k}||\mathbf{B_0}$ with a right-helical antenna. The measurements agree reasonably well with the theory for an $m = +1$ mode but not for an $m = -1$ mode. Axial profiles of the wave fields are shown in Fig. 26[64]. The wave amplitude oscillates downstream from the antenna. This was found to be compatible with the expected beating of two modes with different values of k, as shown by the theoretical curve.

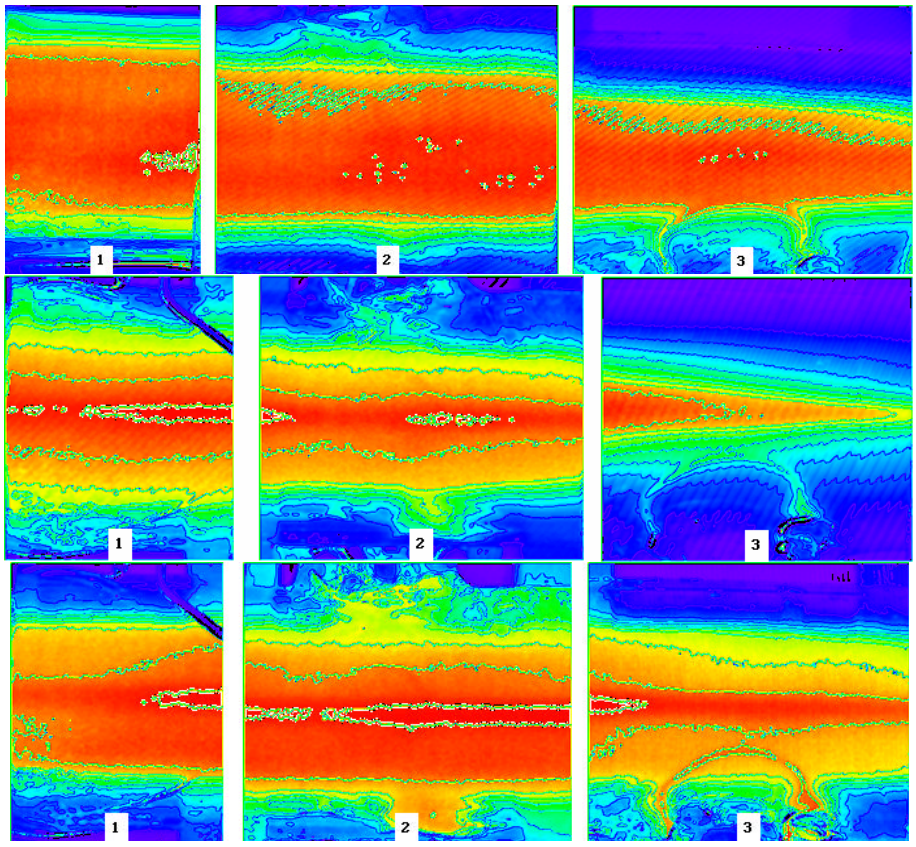

Fig. 24. Side views of a 10-cm diameter helicon discharge. The top row is for a Nagoya Type III; the second row is for an mm = –1 helical, and the bottom is for an $m = +1$ helical antenna. (Ref. 71)

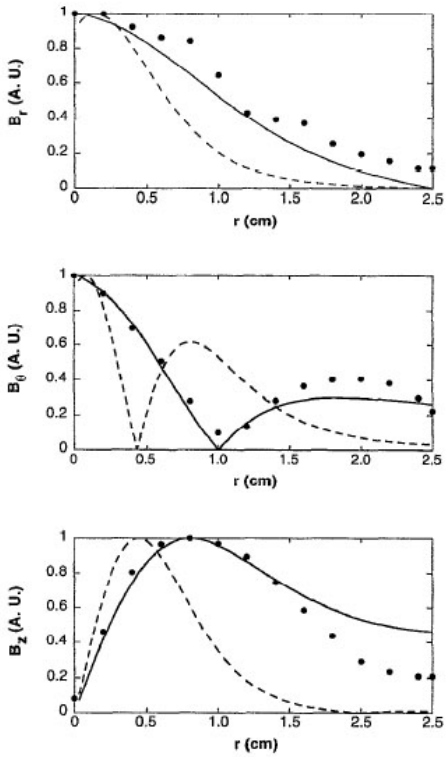

Fig. 25. Example of comparison of experiment (dots) with theory (lines) for $B_z(r)$. The solid line is for the $m = +1$ mode, and the dashed line for the $m = -1$ mode (Ref. 72). Reproduced with permission from Phys. Plasmas **2**, 1084, Copyright 1995, AIP Publishing LLC.

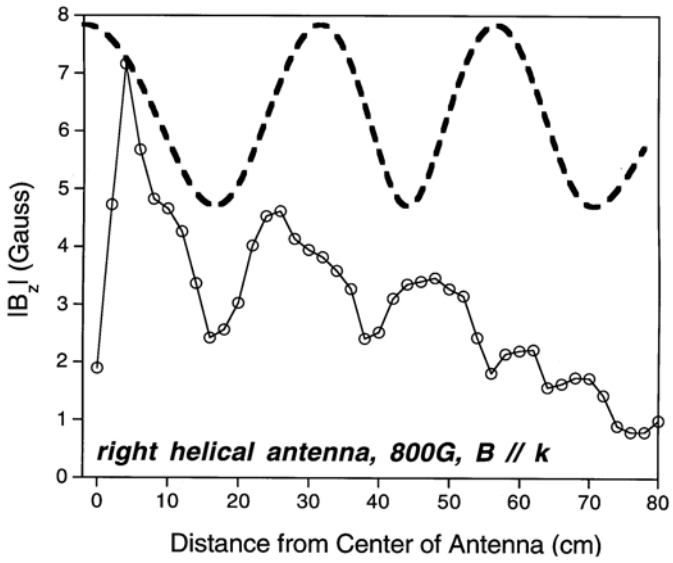

Fig. 26. Example of comparison of experiment (dots) with theory (dashed lines) for $B_z(z)$ (Ref. 73). Reproduced with permission from Phys. Plasmas **2**, 4094, Copyright 1995, AIP Publishing, LLC.

X. More recent experiments

After these initial forays, research into helicons expanded worldwide. Samples of the experimental efforts follow.

1. Experiments by Shinohara et al. A large helicon machine was built in Japan by S. Shinohara et al.[74, 75] It is shown in Fig. 27. Properties of the plasma have been studied with

changes in the B-field uniformity and endplate conductivity[76]; different types of antennas[77], including flat spirals tapped at various points and arrays of $m = 0$ loop antennas[78,79,80]; and different sizes and aspect ratios of the discharge column, including diameters as small as 1 cm[81]. By biasing concentric-ring antennas, the radial electric field and plasma profile can be changed to study instabilities[82,83,84]. The extensive studies of helicons under disparate conditions by Shinohara and collaborators have demonstrated the versatility of helicons for various applications.

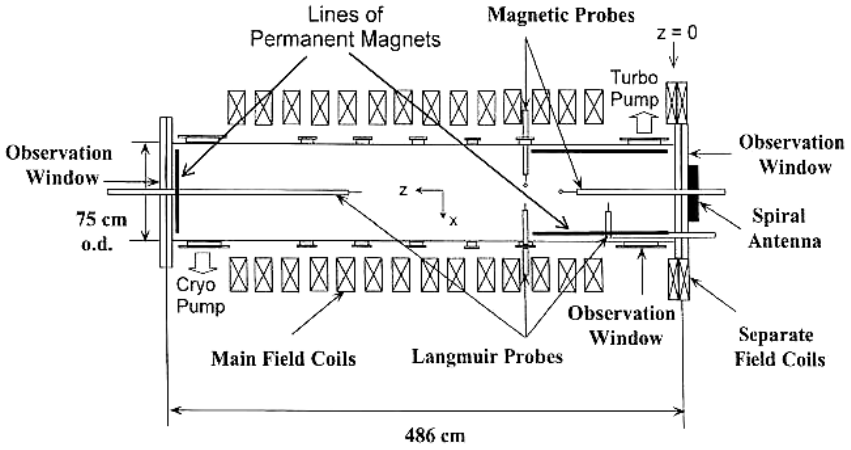

Fig. 27. A large helicon machine (courtesy of S. Shinohara).

2. Experiments by Scime et al. Earl Scime has probably been the most active promoter and researcher in helicon physics. The breadth of activity on helicons can be seen in his summary[85] of papers presented in a mini-conference that he organized at the 2007 meeting of the APS Division of Plasma Physics. In his own group at West Virginia University, experiments are mostly done on the HELIX machine[86], shown in Fig. 28. The antenna is on a 10-cm diam Pyrex tube leading into a 15-cm diam metal chamber, and then into the large expansion chamber. A

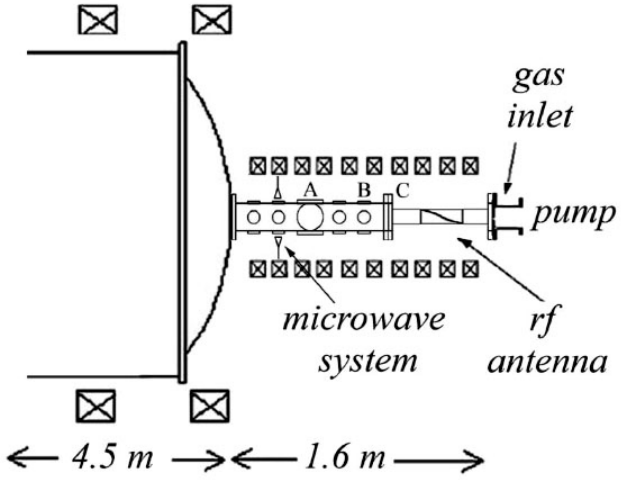

Fig. 28. The HELIX helicon source at West Virginia Univ. (Ref. 86).

distinguishing feature of this experiment is the Laser Induced Fluorescence (LIF) system, which can measure the perpendicular ion temperature. This was found to be much higher than expected from equilibration with neutral atoms[86,87], indicating a source of ion heating. This source was

conjectured to be a parametric decay instability in which the RF generated a lower hybrid wave and an ion acoustic wave, and the latter was the ion heating mechanism[88].

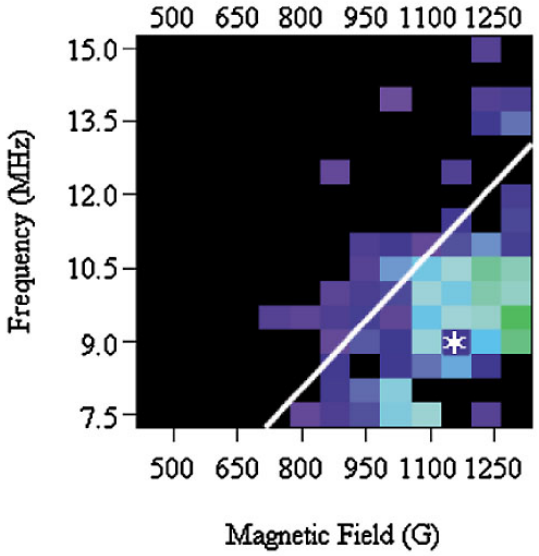

Fig. 29. Evidence of high ion temperatures below the lower hybrid frequency (line). Ref. 87.

A recent experiment in this group had two special features. First, it was done in krypton, a expensive gas that is rarely available. Second, a new diagnostic, two-photon absorption laser induced fluorescence, was developed to measure the neutral density profile. One result was the finding that, as the B-field was increased from 600G to 1200G, with power increasing from 600W at 13MHz to 800W at 11Mhz, the plasma changed from a gently peaked profile with uniform neutral density to a sharply peaked profile with total neutral depletion on axis. This helps to justify the conjectured explanation for the Big Blue Mode mentioned in Sec. IX.

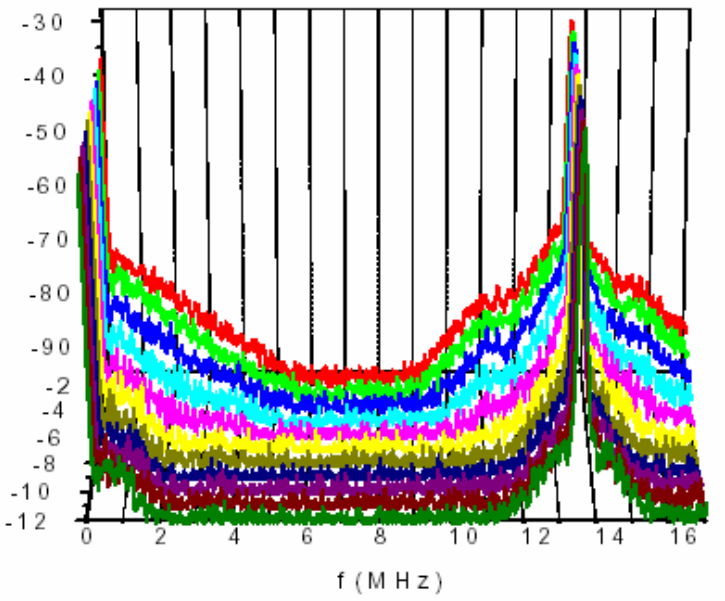

Fig. 30. Electrostatic field of the TG mode and its decay into ion waves, as RF power is raised (Ref. 88).

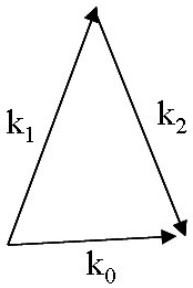

$$\omega_0 = \omega_1 + \omega_2$$
$$\mathbf{k}_0 = \mathbf{k}_1 + \mathbf{k}_2$$
$$\mathbf{k}_{\perp 0} = \mathbf{k}_{\perp 1} + \mathbf{k}_{\perp 2} \approx 0, \quad \mathbf{k}_{\perp 1} \approx -\mathbf{k}_{\perp 2}$$

Fig. 31. Decay scheme of Fig. 30. k_0 is the helicon wave, and k_1 and k_2 are the TG wave and an ion acoustic wave.

3. Experiment by Krämer et al. Deposition of RF energy from the TG mode into the plasma was found by Krämer et al.[89, 90] to involve an interesting process involving parametric instabilities. Figure 30 plots the electrostatic field from a capacitive probe, showing sidebands arising from the low-frequency oscillation seen at the left. These ion acoustic waves are created by parametric decay of the helicon wave via the process shown in Fig. 31. The ion waves were shown to grow nonlinearly with RF power. Though the phases and other details of the parametric interaction were measured in detail, it is not clear whether this process is important in the transfer of RF energy into the plasma. Calculations for this experiment were done by Fischer[91]. Incidentally, this experiment used a vertical helicon discharge, in which the magnetic coils were stacked vertically, greatly simplifying the coil mounts.

4. Experiments by others

Helicon experiments have been done all over the world. Only a sampling can be given here. In Japan, Sakawa et al., working with T. Shoji[15] and others, studied helicon production with $m = 0$ loops[92,93,94]. This work eventually led to the commercial MØRI machine in Sec. XIII. As shown in Fig. 6, the $m = 0$ mode has a completely different structure from the asymmetric modes. Also from Japan, the work by Shinohara was covered above. Y. Mori et al.[95] successfully excited helicons in hydrogen both above and below the lower hybrid frequency. They also saw a low-field peak (Sec. VIII).

In Korea, Yun, Kim, and Chang have studied helicons near the lower hybrid frequency[96], excited the $m = \pm 1$ and ± 2 modes[97], and measured the ionization efficiency of helicons[98]. Yun et al. have found a density rise near the LH frequency with m = 0 antennas[99]. Kim and Chang measured the ion energy distributions[100], and Eom et al.[101,102,103] have generated helicons at high frequencies up to 180MHz.

In Australia, helicons were also used to create the plasma in toroidal fusion experiments[104,105]. A new large helicon source MAGPIE has been built at ANU and Chang et al.[106] have separately controlled and measured the radial and axial profiles of the plasma and the waves.

In Germany, a large helicon machine VINETA[107] was built at Greifswald. It had four identical modules, each with eight large magnet coils. Detailed profiles of the plasma the wave properties were obtained in both helicon and capacitive modes.

In France, Corr et al. observed ion acoustic waves as sidebands of the RF frequency[108] and created stable helicon discharges in Ar/SF_6 mixtures[109]. Further in connection with plasma processing, Petri et al.[110] measured the oxygen from the walls in an SF_6 helicon plasma.

In India, helicons have caught the interest of many physicists. Sahu et al.[111,112] showed that this interest had reached beyond the major institutes. Ganguli et al.[113] calculated the helicon wave fields, with damping, for various levels above the minimum of a curve in Fig. 1. The "F" which they observed[114] in experiment is a more gentle potential drop than is seen by others. Paul and Bora[115] used helicons for RF current drive in a torus. The new twist is that the current is driven nonresonantly via helicity injection. Anitha et al.[116] studied the trapping of helicons in a magnetic bubble, a mirror trap with B ≈ 0 at the center. Tarey et al.[117] built a helicon source 15 cm in diameter and 160 cm long in which they studied axial particle confinement with magnetic mirrors and electric barriers. Barada et al.[118] observed low-field helicons near electron cyclotron frequency in a 10-cm diam chamber with a helical $m = +1$ antenna at the center. The electron cyclotron peak at 5G was observed on the "backward" side of the antenna but was very small on the "forward" side.

In the United States, the large helicon machine of N. Hershkowitz, shown later in Fig. 34, was the centerpiece of the Wisconsin NSF Center for Plasma Aided Manufacturing. Among the many papers from this program are 1) a study of neutral pumping by the helicon plasma[119] and observation of electron beams accelerated by the waves[120]. In the EECS Department at Wisconsin, John Scharer' group built a 10-cm diam, 122 cm long helicon source[121] and measured the plasma and wave profiles in both uniform and nonuniform B-fields. A major contribution was a 2D code for helicons, similar to the HELIC code[23], written by Mouzouris[122]. At the Univ. of Illinois, Urbana, Reilly and Miley[123] have used magnetic probes to see the three-dimensional structure of a helicon wave. They found deviations from the azimuthal symmetries that are usually assumed.

At the University of California San Diego, G. Tynan has constructed the large machine CDCX[124] (Controlled Shear Decorrelation Experiment) to simplify instability and transport effects in tokamaks to linear geometry. The helicon source is 10 cm in diameter, with a two-loop $m = 0$ antenna driven up to 1500W at 13.56 MHz, and injects plasma into a 3m long chamber with a field of 1000G. At the far end, a series of concentric rings is used to measured the radial plasma transport. The plasma is subject to drift-wave instabilities peaking at 3-cm radius at a frequency of ~25 kHz. The plasma turbulence is characterized with correlation measurements, leading to a turbulent Reynolds stress $\langle (d/dr)(\tilde{v}_r \tilde{v}_\theta) \rangle$. According to P. Diamond[125], this should drive a poloidal flow, which was indeed seen and measured[126]. In collaboration with Scime (cf. Sec. X), laser induced fluorescence was brought to the experiment, and this sheared poloidal flow was directly measured, along with the perpendicular ion temperature[127]. This brief summary cannot do justice to the sophistication of this experiment.

On the theoretical side, recent contributions from the U.S. include the possibility of very low frequency helicons in radially localized modes, predicted by Breizman and Arefiev[128] and a detailed treatment of charge exchange collisions with realistic ion orbits by the same authors[129].

XI. Conundrums and insights

Throughout the history of helicons numerous problems have arisen in the behavior of these discharges. As one mystery was solved, another would appear. It is like the peeling of an onion; each layer reveals another one underneath. Here we shall describe some of these layers.

1. Why does the amplitude oscillate along the cylinder?

The solution was given in the previous section: it is due to the beating of simultaneous excitation of waves with two values of k.

2. Why is a right-helical antenna better than a left one?

HELIC calculations show a higher value of plasma resistance R for the $m = +1$ mode than for the $m = -1$ mode. If by right-helical antenna we mean one that launches an $m = +1$ mode in the "downstream" direction away from an endplate, this expected since the mode patterns of Fig. 5 show stronger fields at the edge for the +1 mode.

3. What causes the high ionization efficiency?

This was found to be due partly to the TG mode, whose fields are necessary to satisfy the boundary conditions at the confining radial wall.

4. Why does an endplate behind the antenna increase n?

This is caused by the reflected wave, as shown in Fig. 18.

5. Why is the density peaked at the center?

The density has to decrease radially so that Maxwellian electrons can create an E-field pointing outwards, pushing the ions out. If the density were low on axis, ions would be pushed inwards by the E-field and can only escape to the endplates at their slow thermal speeds. The central density would then build up until it is highest there.

6. Why is the ion temperature so high?

E. Scime *et al.* have contributed extensively to the science of helicons. One of their discoveries is that the ion temperature is much higher than would be expected from thermal equilibrium with the neutral gas. This was attributed to ion Landau damping at the lower-hybrid frequency.

7. Why is a half-wavelength antenna better than a full?

It would seem reasonable that a full-wavelength helical antenna would have a narrower spectrum and would couple better to the plasma than the usual half-wavelength antenna. But it was found[130] (Fig. 27) that the opposite is true. This has not yet been explained.

8. Why is the discharge sometimes hard to ignite?

When an RF pulse is applied to the antenna, a few electrons from the cosmic ray background are accelerated, strike neutral atoms, and cause an avalanche which starts the ionization process. At low pressures and small diameters, ignition may not occur; and then it is necessary to start the plasma at high pressure, 30-40 mTorr, say, and then reduce to the operating pressure. Breakdown is more easily achieved at 27 MHz than at 13 MHz.

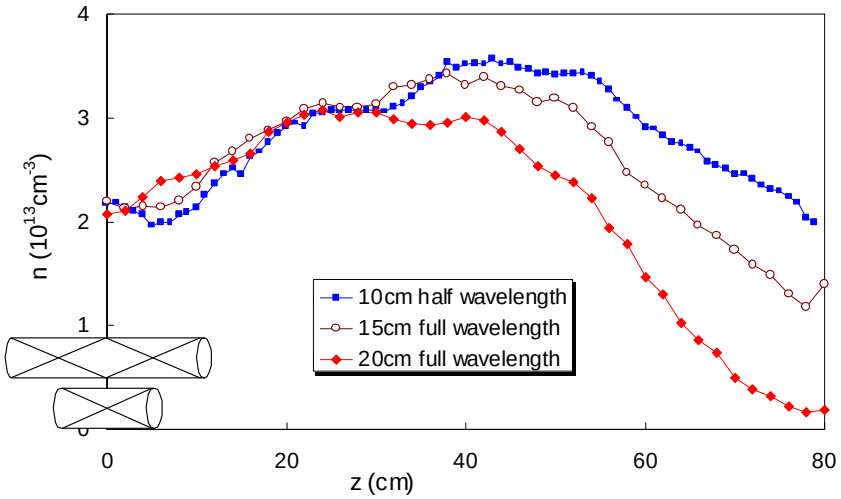

Fig. 27. Density profiles $n(z)$ with full- and half-wavelength helical antennas centered at $z = 0$ (Ref. 130). Reproduced with permission from JVSTA **11**, 1165, Copyright 1993, American Vacuum Society.

8. Electric fields

The antenna mechanism of Fig. 7 shows that *electrostatic* fields are an essential element of this *inductive* discharge. In the absence of full scans of E-field in a helicon discharge, we show HELIC calculations of these fields. Figure 30 shows radial plots of |B| and |E| for the H and TG modes separately. The H mode has |B| slightly peaked on axis and |E| slightly peaked at the edge, while the TG mode has both strongly localized to the edge.

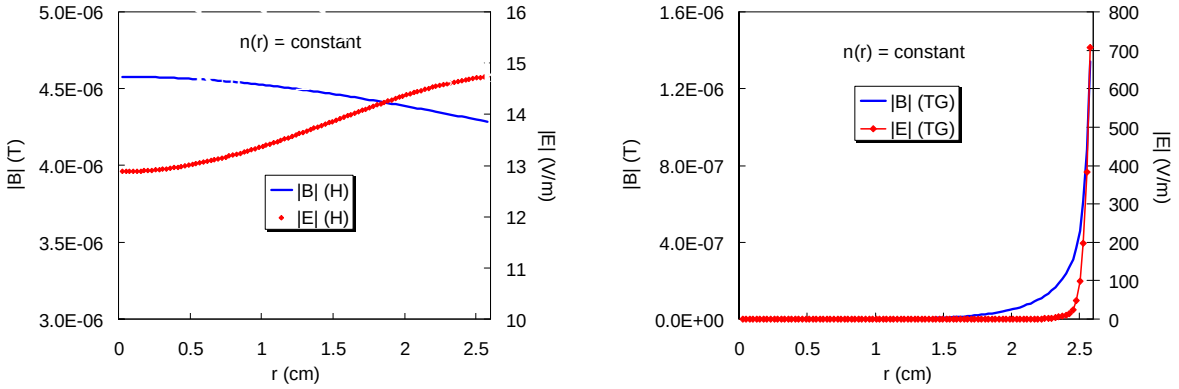

Fig. 30. Computed $|B|(r)$ and $|E|(r)$ for the H and TG modes in a uniform plasma with $B_0 = 0.1$T at 13.56 MHz, $n(0) = 10^{12}$ cm^{-3}, $KT_e = 3$ eV, $p = 15$ mTorr of argon, and an $m = 1$ half-helical antenna carrying 1A of current. Note the suppressed zeros.

Although it would seem that the E-field, reaching 700V at the edge, is dominant, it is the rf magnetic field that has most of the wave energy, as shown in Fig. 31. Thus, a helicon discharge is still quite different from a capacitive discharge, in spite of the fact that the rf energy enters mainly through electric fields at the edge.

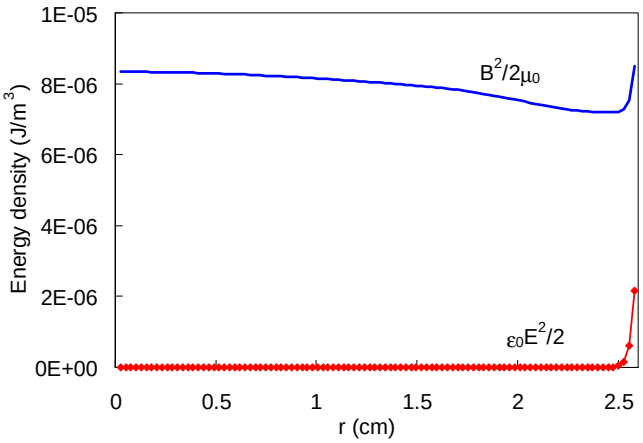

Fig. 31. Energy densities of the RF B- and E-fields (not including B_0), plotted on the same scale, for the same uniform plasma as in Fig. 28.

9. Instabilities

Most helicon discharges are long enough to be subject to drift-wave type instabilities, which are driven by the necessary radial pressure gradient. Indeed, Light et al.[131] have seen both discrete modes and turbulence in the 10-kHz regime, as seen in Fig. 32A. The nonlinear limit of the amplitudes increased with B_0 and their growth rates decreased with ion mass (Fig. 32B).

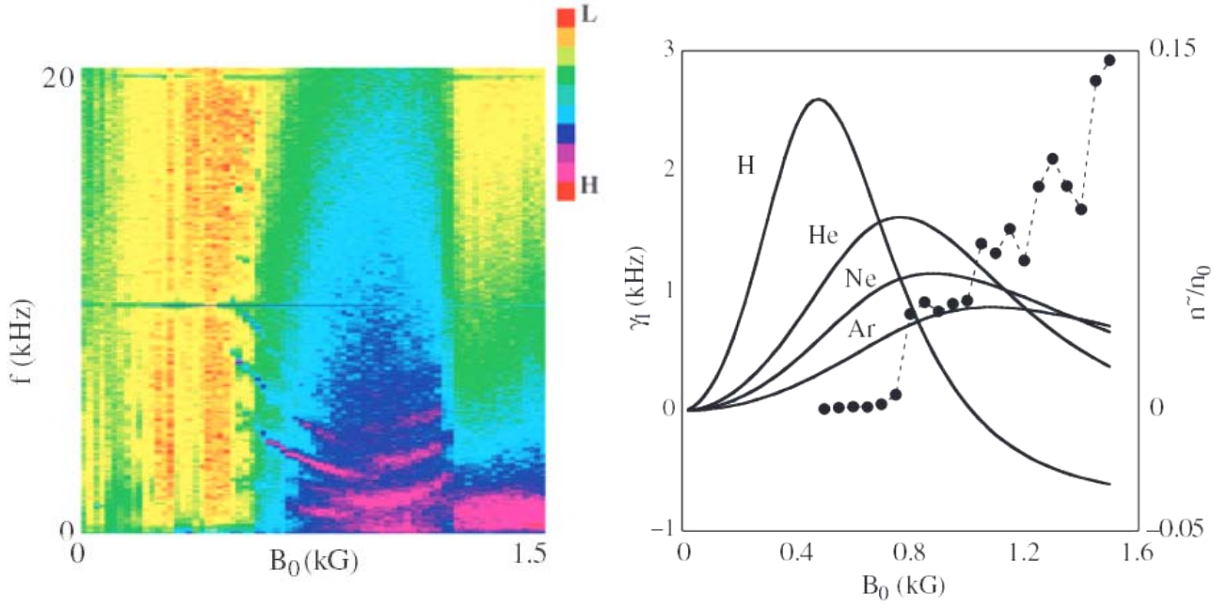

(A) (B)

Fig. 32. (A) Frequency spectrum vs. B_0 in a neon helicon discharge and (B) measured growth rates γ_I in various gases (left scale) and fractional instability amplitude (right scale) [Ref. 131].

Tynan et al.[132] have measured the anomalous transport in the sheared azimuthal $\mathbf{E} \times \mathbf{B}$ flow in a large helicon discharge (cf. Sec. X-4) As expected, the particle flux in the turbulent plasma is largest at the radius where *dn*/*dr* maximizes.

Drift instabilities have long wavelength parallel to $\mathbf{B}_0$. They cannot arise in short plasmas. This has been confirmed by Chen[133] in a small helicon source 5 cm in diameter and 5 cm long. A trace of the ion saturation current to a probe is shown in Fig. 33. No low-frequency oscillations can be seen.

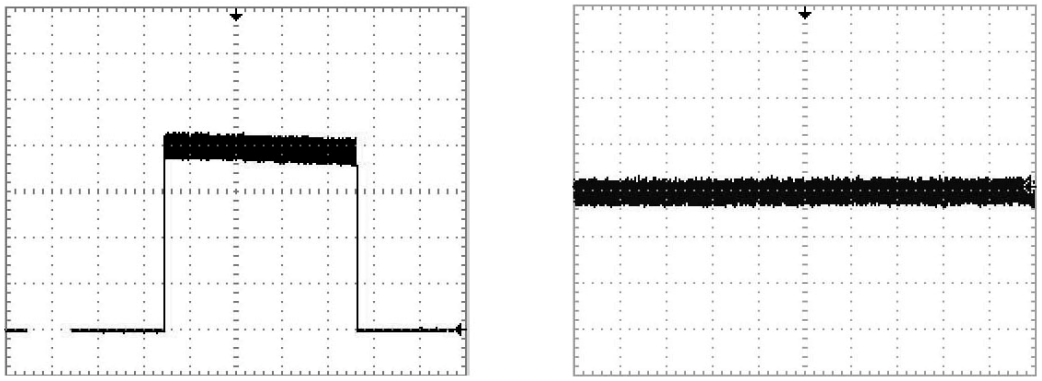

(A) (B)

Fig. 33. Oscilloscope traces of ion saturation current to a probe in a small helicon discharge. Sweep speeds are (A) 1 sec/div and (B) 5 μs/div. The hash is pure 27.12 MHz RF pickup (Ref. 133). Reproduced with permission from Phys. Plasmas **19**, 093509, Copyright 2012, AIP Publishing LLC.

XII. Versatility

During the past three decades of intense activity on helicon discharges, many types of machines have been built, large and small. Shinohara has built a large number of devices ranging from 2 cm to 74 cm in diameter[134,135,136]. Many experiments on DC electric fields in the

plasma have been done by applying voltages to split endplates[137,138]. Figure 34 gives an idea of what a large helicon discharge looks like[139]. The coils are 25 cm in inner diameter. Another large university installation is the HelCat machine of M. Gilmore[140] at the Univ. of New Mexico, shown in Fig. 35.

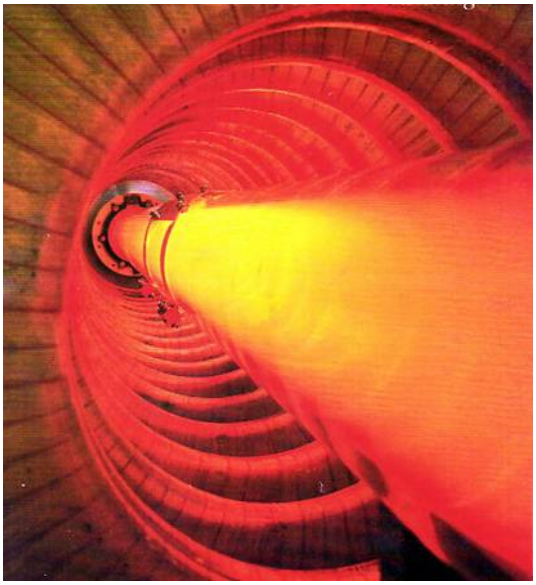

Fig. 34. A large helicon source at the Univ. of Wisconsin (Ref. 139).

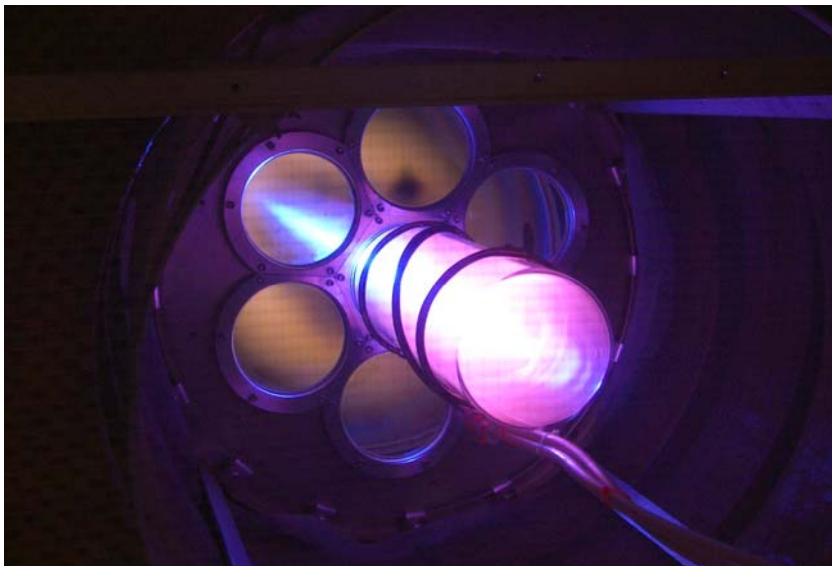

Fig. 35. The HelCat helicon machine (Ref. 140). Picture by the author.

An even larger helicon is being built for a spacecraft intended for travel to Mars, the VASIMR (Variable Specific Impulse Magnetoplasma Rocket) being built by Chang-Diaz[141]. A diagram is shown in Fig. 36. The plasma is further heated by ion cyclotron resonance heating. The possibility of parametric instabilities has been raised by Boswell *et al.*[142]. The need for high-density plasmas for this purpose has inspired Squire, Winglee *et al.*[143,144,145] to produce high-power, high-density helicons.

At the other extreme, a mini-thruster can be made with a 5 cm × 5 cm helicon tube and a permanent magnet. A picture of a prototype[146] of this proposed device is shown in Fig. 37. The simplicity of such single-loop antennas has appealed also to Shamrai[147] and to Carter and Khachan[148]. The large chamber in Fig. 37 has small permanent magnets covering the outside wall to help confine the plasma. This method had been used earlier by Charles[149].

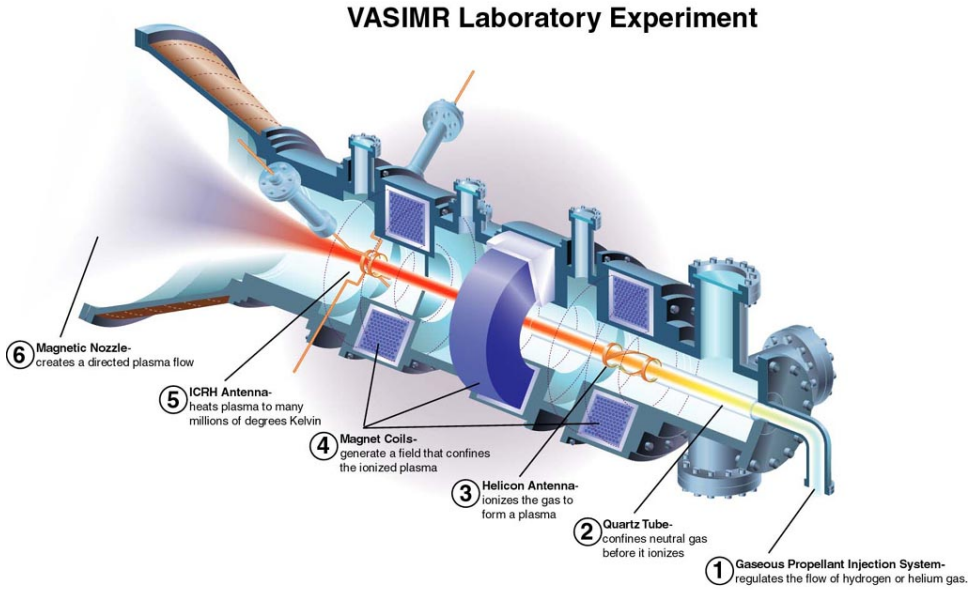

Fig. 36. Diagram of the VASIMR (Ref. 150)

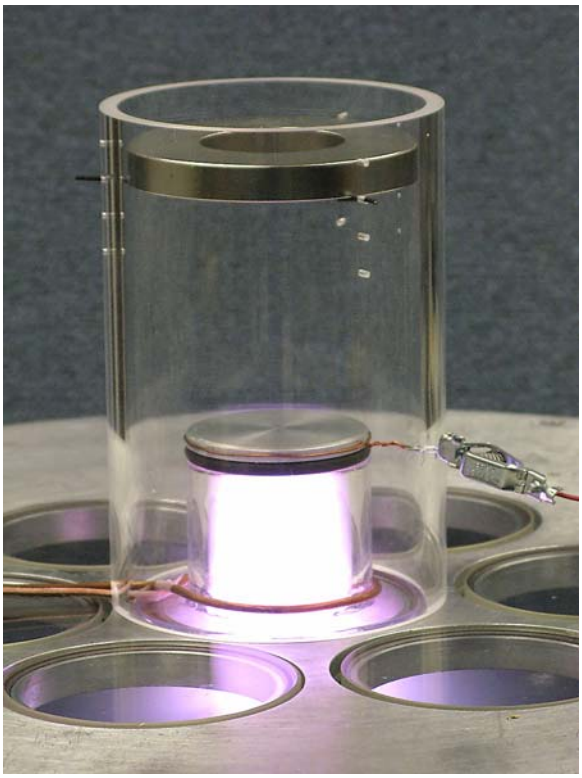

Fig. 37. Photo of a 5-cm diameter helicon source using the remote field of a permanent magnet (Ref. 146).

Helicon sources have also been used to inject plasma into toroidal chambers. For instance, Loewenhardt *et al.* used a helicon source to fill a toroidal heliac[151] fusion confinement device, and Sakawa et al.[152] used helicons to fill a torus with hydrogen.

XIII. Applications

A. Plasma processing. The most obvious use of helicon sources was for etching and deposition in the manufacture of semiconductor circuits. The standard systems are capacitively coupled plasmas (CCPs) and inductively coupled plasmas (ICPs). CCPs are parallel plates with the silicon wafer mounted on the bottom one. RF on the top plate generates the plasma, and a bias on the bottom plate accelerates ions onto the wafer. CCPs are used mostly for deposition of silicon oxide. ICPs use antennas on a dome above the wafer chuck to generate a plasma without a B-field. Helicon sources would generate higher plasma density and decrease the processing time, but they have not yet been accepted by the semiconductor industry.

The first helicon built for commercial use was that of Benjamin et al.[153] in 1991. This source by Lucas Labs. was compared with ECR sources in three papers by Tepermeister et al.[154,155,156] They found that the Lucas source was not better than an ECR source in etch rate but gave somewhat better uniformity.

A few years later, a company PMT, Inc. was formed in Chatsworth, CA, by R. Conn and G. Campbell, with advice from T. Shoji and the author, to manufacture the MØRI (m = 0 reactive ion etcher) plasma source[157] shown in Fig. 38. This used a two-ring antenna with opposite currents. The B-field was provided by two coaxial coils with the outer one carrying a current in the opposite direction so as to flare out the field, preventing it from reaching the substrate. This source passed "marathon" tests for endurance and was even made into a cluster tool for cleaning, etching, and deposition steps in semiconductor production. The company failed due to a poor business decision.

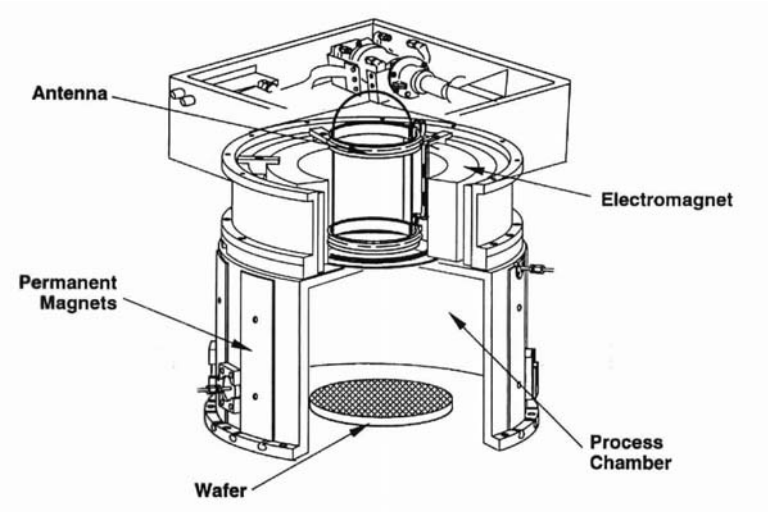

Fig. 38. The MØRI helicon source (Ref. 157). The matching circuit is sketched above it. Reproduced with permission from JVSTA **15**, 2885, Copyright 1997, American Vacuum Society.

At the time, the state of the art was in 300-mm (12-inch) diameter silicon substrates. To cover such an area uniformly with dense plasma, experiments were done with arrays of helicon sources. To produce uniform coverage of the substrate, an array of tubes such as that shown in Fig. 39A was envisioned. The seven tubes would actually be arrayed as in Fig. 40. However, this arrangement would suffer losses to the top flange, as shown in Fig. 39B. To solve this, the B-field must be generated by a large electromagnet covering all the tubes, as in Fig. 41. The

small tubes shown there are prototypes of the tube shown in Fig. 37. Density profiles of this array source, seen in Fig. 42, showed good uniformity over a surface 40 cm in diameter[158]. The 2D plot of the density in Fig. 43 shows no trace of the 6-fold symmetry of the sources. To eject plasma toward a substrate requires allowing the plasma to leave the magnetic field lines. A test of ejection was carried out by X. Jiang in Chen *et al.*[159] Smooth, peaked density profiles were measured downstream, but the densities were low because the field lines that reach the substrate originate from only a small central column of the discharge (Fig. 39B). The rest is lost to the walls.

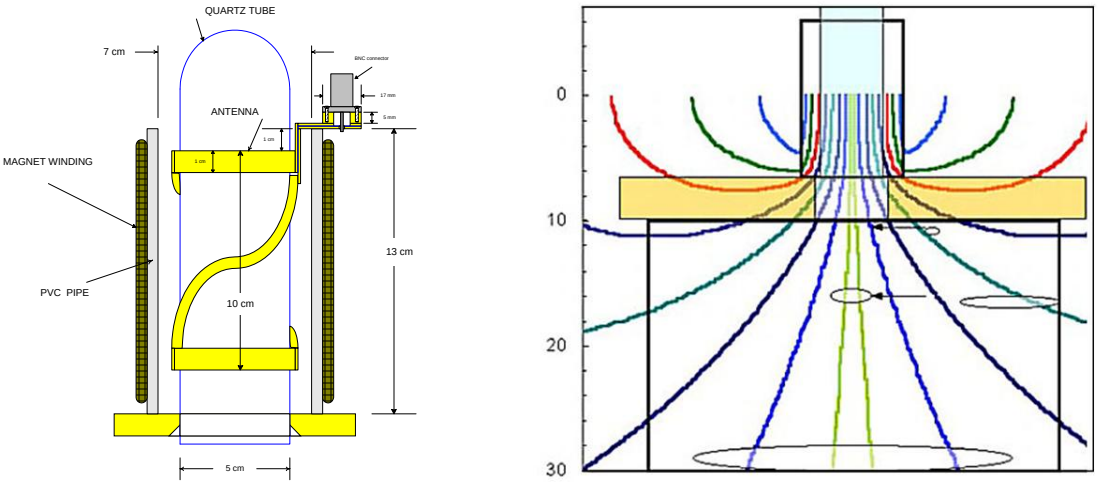

Fig. 39. (A) Diagram of a small helicon source with its own magnet coil and helical antenna. (B) Field lines from this source and the sizes of electron Larmor orbits at various downstream locations (Ref. 159). Reproduced with permission from JVSTA **18**, 2108, Copyright 2000, American Vacuum Society.

The necessity for such a large electromagnet made the device impractical for large-scale manufacturing, and it was not adopted by the semiconductor industry. This constraint has been largely alleviated by the use of permanent magnets. PM helicons will be described in a later section.

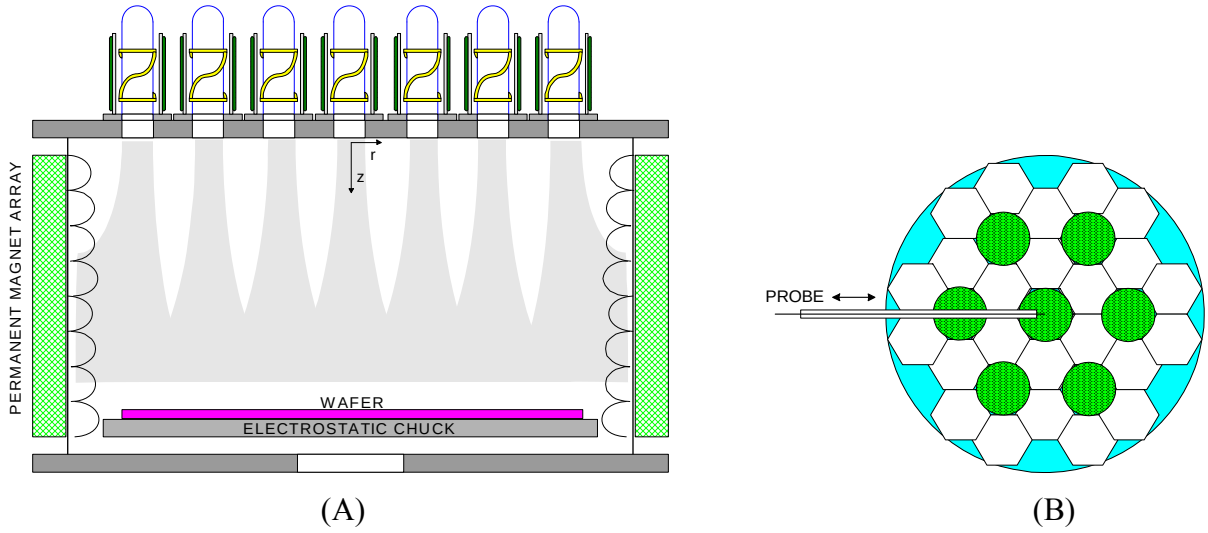

Fig. 40. (A) Proposed array of seven helicon sources. Radial confinement is improved by covering the walls with small permanent magnets. (B) Actual circular arrangement of the seven sources.

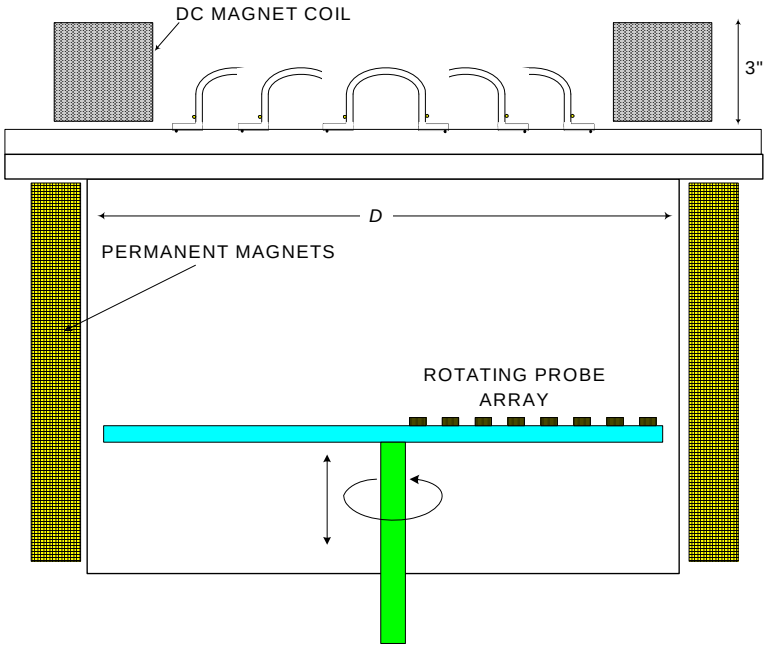

Fig. 41. An array of seven small tubes with a large magnet providing the B-field.

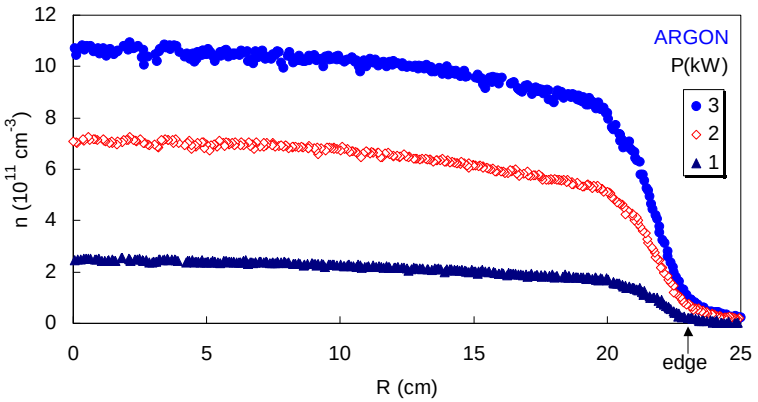

Fig. 42. Radial density profiles in the array source of Fig. 41 (Ref. 158). Similar uniformity also occurred in chlorine plasmas.

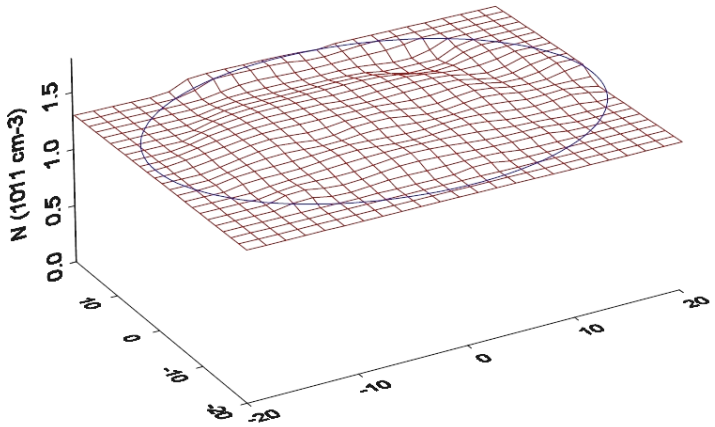

Fig. 43. 2D plot of density from a 7-tube source (Ref. 158; figure omitted from final publication).

B. Spacecraft propulsion. Modern satellites boosted into space use ejection of ions, usually xenon, to achieve the proper orbital velocity. These thrusters are of two types. Gridded ion thrusters create a plasma by accelerating electrons from a thermionic emitter toward an anode. A grid then holds back the electrons while another grid accelerates the ions to high velocity in the exhaust. Electrons are emitted from a external source to neutralize the charges of the ejected ions, keeping the spacecraft from charging up. Hall thrusters also accelerate the ions by applying an electric field, but the electrons are held back instead by a DC magnetic field. An external electron source is still needed to neutralize the ion beam. Helicon thrusters eject a neutral plasma, both ions and electrons, and no neutralizer is necessary. Straightforward application of helicons to Hall thrusters would require helicon waves in an annular geometry. This configuration has been studied by Yano and Walker[160].

Thrusters are characterized by their specific impulse, measured in seconds, which is their exhaust velocity compared with the velocity of a rock dropped from rest for that many seconds under the earth's surface gravity[161]. A helicon thruster has the advantage that ions are accelerated by a sudden drop in space potential, called a "double layer", in the plasma ejected by the source. The double layer is simply a sheath in space. It is well known that if monoenergetic ions are accelerated to the "Bohm velocity", which is just the acoustic velocity $c_s = (KT_e / M_i)^{1/2}$, the ion density in a falling potential will be larger than the Maxwellian electron density, and this will cause the potential to fall further, creating the sheath on a wall[162]. This can also occur in free space, where electrons will rush in to cancel the ion charge, creating a double layer (Fig. 44). C. Charles has written a review of double layers[163].

There is a large literature on this complicated phenomenon. To give the reader an idea of why it occurs, we give a simplified calculation[164] of the location of the double layer when the B-field lines are diverging, as in Fig. 45. For Maxwellian electrons, the plasma density is given by

$$n_e = n_0 e^{-\eta}, \quad \text{where} \quad \eta = -\mathrm{e}V/KT_e . \tag{11}$$

The Bohm energy is

$$v_{is} = c_s = (KT_e / M)^{1/2} \therefore W_{is} = \tfrac{1}{2} M v_{is}^2 = \tfrac{1}{2} KT_e . \tag{12}$$

To gain this energy, ions must have been accelerated by a sheath potential $\eta_s = \tfrac{1}{2}$.

$$\therefore \quad \eta_s = \tfrac{1}{2}, \quad n_s / n_0 = e^{-1/2}, \quad B / B_0 = n / n_0 = (r_0 / r)^2, \quad r / r_0 = e^{1/4} = 1.28 . \tag{13}$$

A single layer (an ion sheath) forms where r has increased 28%. In the absence of a wall, electrons will be attracted to the positive charge and shield it, forming a double sheath.

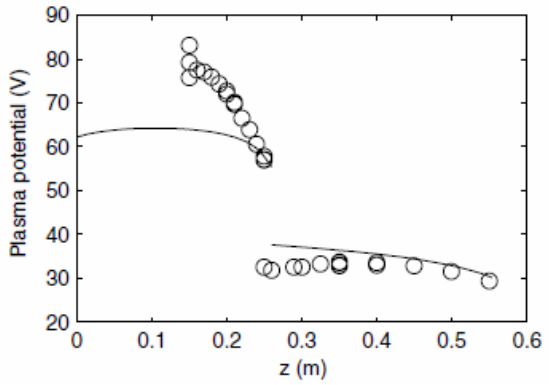

Fig. 44. Observation of the potential jump associated with a double layer in free space (Ref. 163).

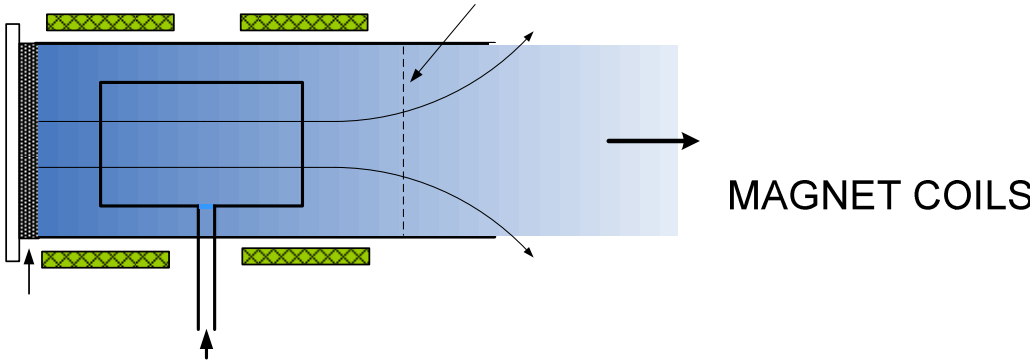

Fig. 45. Location of the double layer downstream of a helicon discharge.

On the subject of thrusters, there are several papers on the shape of the plume, or magnetic nozzle, of plasma emitted[165,166,167,168]. These details are outside the scope of this paper. Upon satellite re-entry, a plasma of density $\approx 10^{17} m^{-3}$ is formed by the nosecone striking the atmosphere. Lemmer et al.[169] have simulated these plasma conditions with a helicon source.

XIV. Permanent-magnet helicons

The DC magnetic field that helicons require has impeded their acceptance in industry. It is possible, however, to use permanent magnets to produce long, quasi-uniform B-fields. This may be an important development in helicon design for such practical applications as semiconductor etching and spacecraft propulsion. Takahashi[170] has used straight PMs, but most work has been done by Chen[27] with annular magnets. That system will serve as an example for what can be done with PMs. When polarized vertically, the B-field of ring magnets has a stagnation point not far below the magnet, and the field below this point, though much weaker than that inside the hole, is fairly uniform and extends to infinity (see Fig. 47B later). Neodymium (NeFeB) magnets have fields above 1T inside, and even in the remote field below the stagnation point a field of 30-200G is available for helicon experiments.

INSULATOR RF

A. B-field design. The field patterns of various ring magnet designs with different numbers of rings and different spacings between them were computed, as shown in Fig. 46; but there was no advantage over a single ring. The final design suitable for coverage of a 5 cm × 5 cm tube is shown in Fig. 47A.

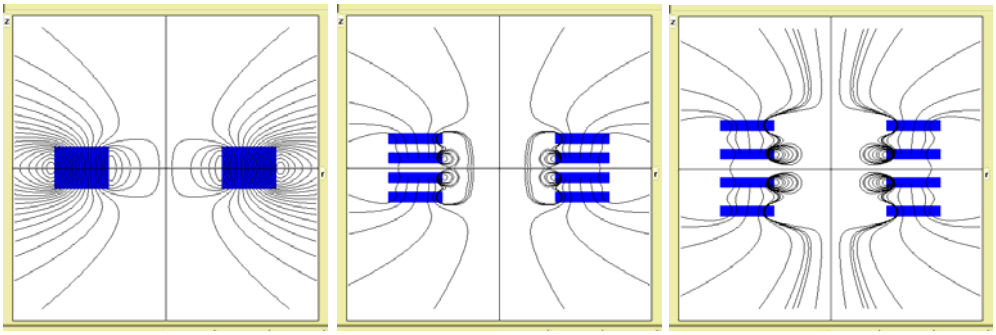

Fig. 46. Examples of field patterns from different magnet arrays.

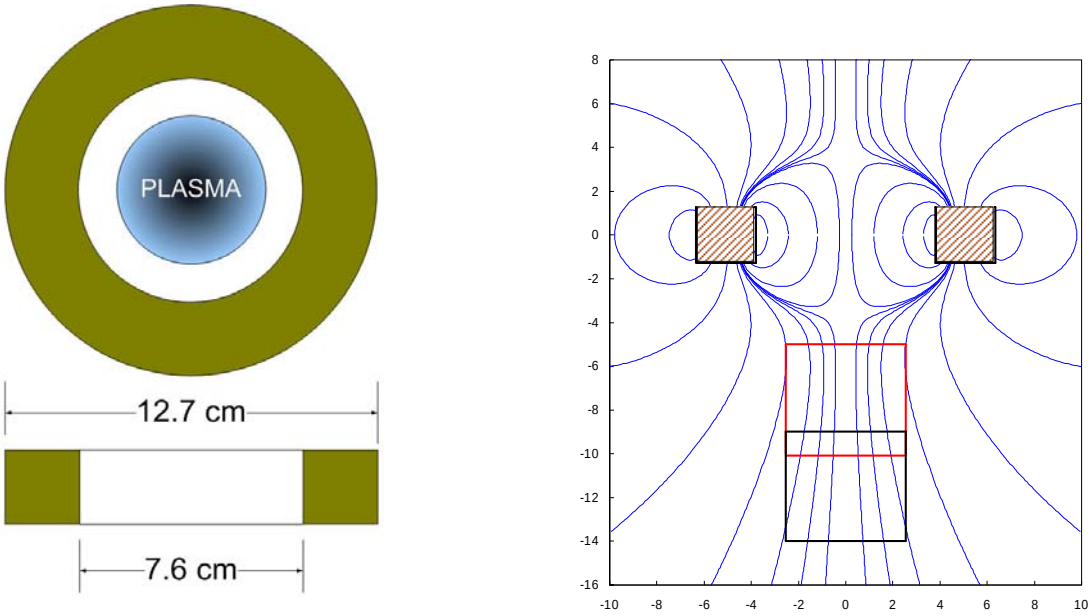

Fig. 47. (A) The designed magnet. (B)Field lines of the magnet. The squares show two possible positions of the discharge tube in the remote field.

B. Tube design. The diameter and length of the discharge tube were determined by computing the plasma resistance R with the HELIC code. The results were organized in matrices showing the variations with tube radius and length, RF frequency, gas pressure, and the top plate material. The final design is shown in Fig. 48.

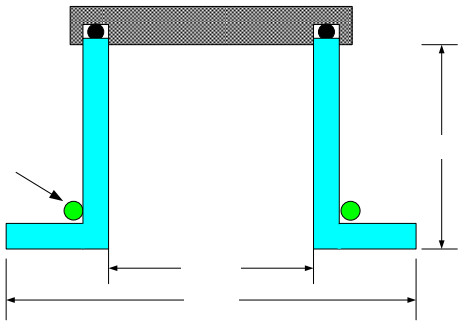

Fig. 48. Final design of the discharge tube.

C. Performance. The source of Fig. 47B has been used to inject plasma to fill a large experimental chamber, and extensive measurements of the plasma downstream have been made[171]. Figure 49 shows density profiles there, following normal collisional diffusion. Figure 50 shows details in Port 1, just 6.8 cm below the source. The $n(r)$ curve is the same as that in `. The KT_e curve shows two peaks due to the TG mode. The plasma (space) potential V_s is shown by dots as measured from the "knee" of Langmuir probe traces and agrees reasonably well with V_s calculated from the Boltzmann equation, knowing n and T_e (line).

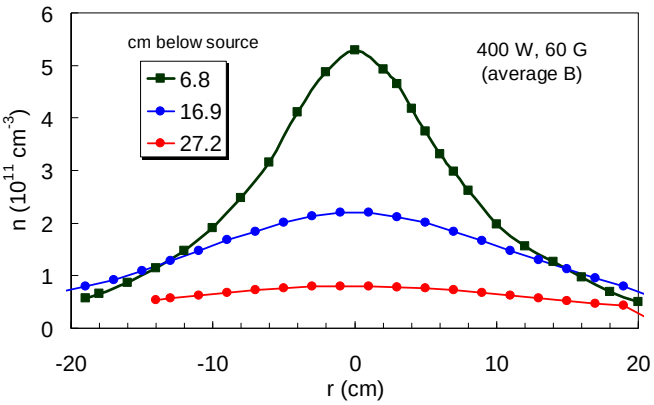

Fig. 49. Radial density profiles downstream from the source of Fig. 47. Reproduced with permission from Phys. Plasmas **19**, 093509, Copyright 2012, AIP Publishing LLC.

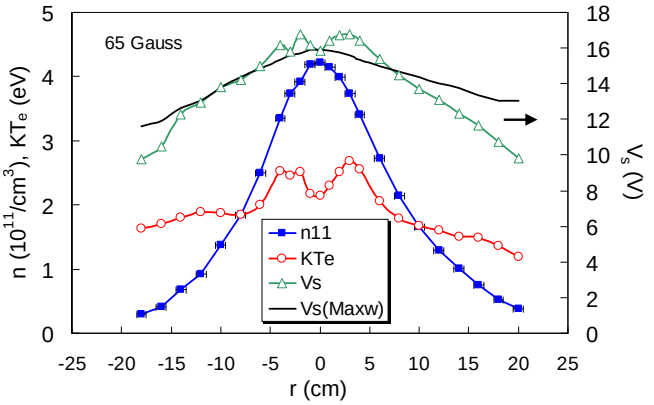

Fig. 50. Radial profiles in Port 1 (Ref. 146) at 400W. Density and KT_e are both shown on the left-hand scale, while space potential V_s is shown on the right-hand scale. Reproduced with permission from Phys. Plasmas **19**, 093509, Copyright 2012, AIP Publishing LLC.

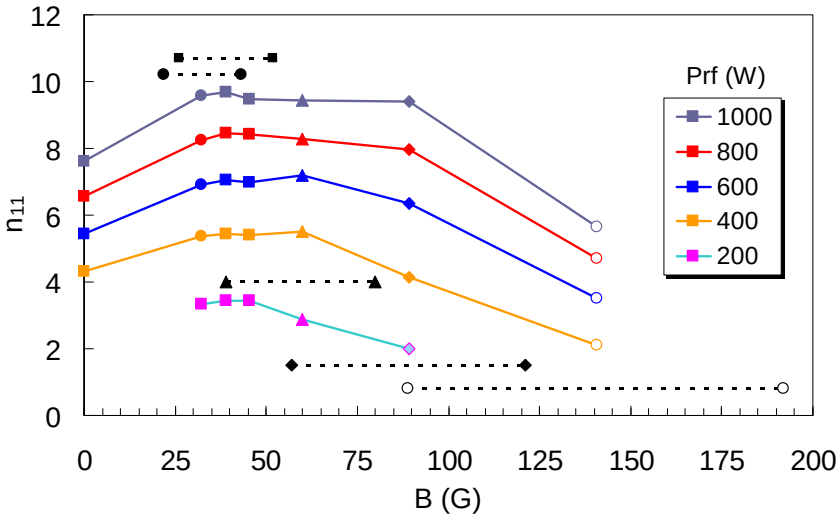

Fig. 51. Peak density in Port 2, 16.9 cm below the tube, *vs.* B_0 and P_{rf} (Ref. 146). The dashed lines indicate the range of B-field within the 5-cm height of the tube. Each dashed line corresponds to the curve with the same symbol above or below the center of the line. Reproduced with permission from Phys. Plasmas **19**, 093509, Copyright 2012, AIP Publishing LLC.

Figure 51 shows peak density 16.9 cm below the source *vs*. B-field and RF power. The density does not rise monotonically with B_0 because of insufficient power to reach the peaks shown in Fig. 14. The density actually decreases at high B_0 because the discharge falls out of resonance. This graph shows that B-fields no higher than about 30 to 60G are sufficient for applications requiring $n \leq 10^{12}$ cm^{-3}. In that case, the large magnet of Fig. 47 is not necessary and can be replaced by an off-the-shelf Nd magnet such as that in Fig. 37.

D. PM arrays. Plasma processing requires uniform coverage of large substrates with plasma densities of order 10^{10}–10^{11} cm^{-3}. The semiconductor industry is advancing to 400-mm diameter silicon. This presents an opportunity for helicons to penetrate the market. A uniform plasma can be produced by a circular array of small helicon sources such as those shown in Figs. 47 and 48. A diagram of such an array is shown in Fig. 52. A theory by Chen and Curreli[172] shows that sources at the edge, with no center source, can produce a plasma uniform to the center. In roll-to-roll processing, a wide plasma source can be used to treat a substrate moving underneath. Such a helicon source is shown in Fig. 53. The tubes are in two rows and can be arranged either opposite one another or staggered. The RF is fed via Teflon-insulated cables of equal length to each tube. All connections are soldered, since coaxial connectors will arc over with the voltages applied. When ≥400W is applied to each tube in parallel, all will light up equally. The magnet rack and distribution box are shown in Fig. 54. Finally, Fig. 55 shows the helicon array powered from a rectangular 50Ω transmission line in which the center conductor is a copper tube carrying both the RF and the cooling water. The water is connected to the tube in pairs, so that it enters and leaves the system at ground potential on the top and bottom flanges of the transmission line. The plasma uniformity at the bottom of the chamber is ±3%.

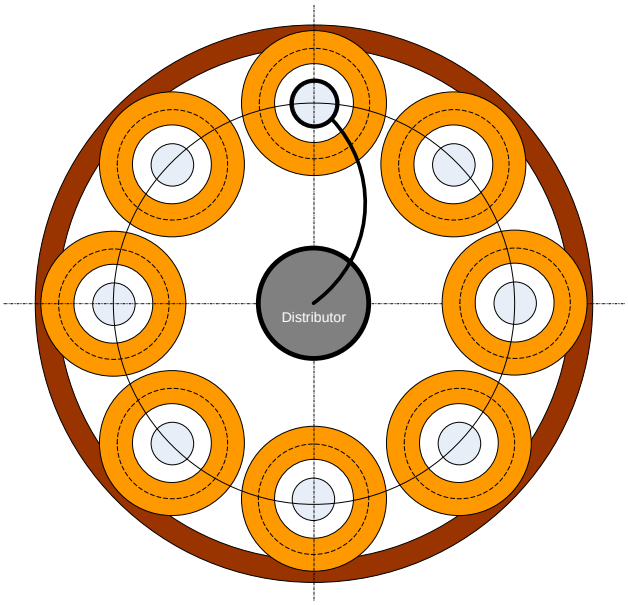

Fig. 52. Design for an 8-tube array source. The power from a matching circuit is fed in parallel to the tubes through a distributor, one arm of which is shown.

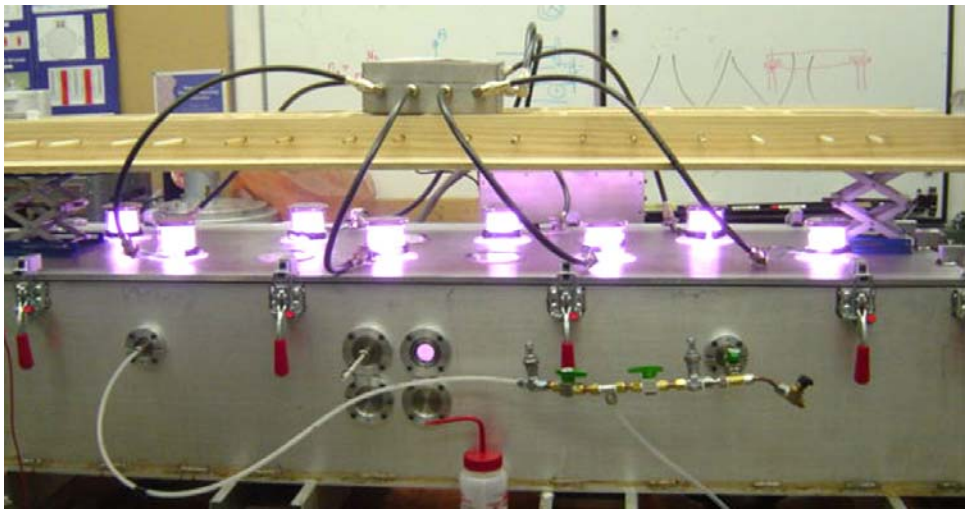

Fig. 53. An 8-tube array of small helicon sources (Refs. 173, 174).

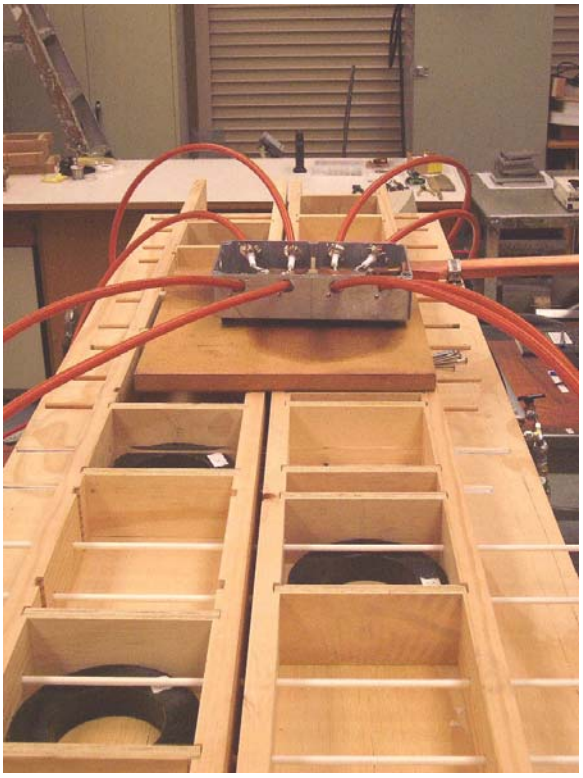

Fig. 54. The distribution box and the magnet rack with movable partitions.

Fig. 55. An 8-tube PM helicon array powered from a rectangular 50Ω transmission line.

XV. Acknowledgments

My quarter-century of work on helicons would not have been possible without the friendship of and collaboration with three theorists: John Dawson (d. 2001), Don Arnush (d. 2003), and Konstantin (Kostia) Shamrai (d. 2013). John contributed the Nagoya Type III antenna mechanism and taught me how to think physically without equations.

REFERENCES

[1] J. A. Lehane, and P.C. Thonemann, Proc. Phys. Soc. **85**, 301 (1965).

[2] Aigrain, P., *Les 'helicons' dans les semiconducteurs*, Proc. Intl. Conf. on Semicond. Phys., Prague (Butterworths, London, 1960), p. 224.

[3] L. Woods, J. Fluid Mech. **13**, 570 (1962).

[4] L. Woods, J. Fluid Mech. **18**, 401 (1964).

[5] C.R. Legendy, Phys. Rev. A **135**, 1713 (1964).

[6] C.R. Legendy, J. Math. Phys. **6**, 153 (1965).

[7] J.P. Klozenberg, B. McNamara, and P.C. Thonemann, J. Fluid Mech. **21**, 545 (1965).

[8] H.A. Bleven and P.J. Christiansen, Aust. J. Phys. **19**, 501 (1966).

[9] H.A. Bleven and P.J. Christiansen, Plasma Phys. **10**, 799 (1968).

[10] H.A. Bleven, P.J. Christiansen, and B. Davies, Phys. Rev. Lett. A **8**, 230 (1968).

[11] R.L. Ferrari and J.P. Klozenberg, J. Plasma Phys. **2**, 283 (1968).

[12] B.J. Davies and P.J. Christiansen Plasma Phys. **11**, 987 (1969).

[13] M.M. Shoucri, Plasma Phys. **11**, 1017 (1969).

[14] R.W. Boswell, Phys. Lett. A **33**, 457 (1970).

[15] T. Shoji, Y. Sakawa, S. Nakazawa, K. Kadota, and T. Sato, Plasma Sources Sci. Technol. **2**, 5 (1993).

[16] G.R. Tynan, A.D. Bailey III, G.A. Campbell, R. Charatan, A. de Chambrier, G. Gibson, D.J. Hemker, K. Jones, A. Kuthi, C. Lee, T. Shoji, and M. Wilcoxson, J. Vac. Sci. Technol. A **15**, 2885 (1997).

[17] B. Chapman, N. Benjamin, C.F.A. van Os, R.W. Boswell, and A.J. Perry, *Plasma dry processing in the helicon reactor*, 12th Symposium on Dry Process, Denki-Gakkai, Tokyo (1991).

[18] ISI Web of Knowledge

[19] R.W. Boswell, Aust. J. Phys. **25**, 403 (1972).

[20] R.W. Boswell, Plasma Phys. Control. Fusion **26**, 1147 (1984).

[21] F.F. Chen, Plasma Phys. Control. Fusion **33**, 339 (1991).

[22] F.F. Chen, *Helicon Plasma Sources,* in "High Density Plasma Sources", ed. by Oleg A. Popov (Noyes Publications, Park Ridge, NJ, 1995), Chap. 1.

[23] D. Arnush, Phys. Plasmas **7**, 3042 (2000).

[24] http://www.seas.ucla.edu/ltptl/presentations.htm

[25] C. Charles, Plasma Sources Sci. Technol. **16**, R1 (2007).

[26] K. Takahashi, K. Oguni, H. Yamada, and T. Fujiwara, Phys. Plasmas **15**, 084501 (2008).

[27] F.F. Chen, Phys. Plasmas **19**, 093509 (2012).

[28] W. Li, Y. Ruan, B. Luther-Davies, A. Rode, and R. Boswell, J. Vac. Sci. Technol. A **23**, 1626 (2005).

[29] J.P. Squire, F.R. Chang-Diaz, T.W. Glover, V.T. Jacobson, G.E. McCaskill, D.S. Winter, F.W. Baity, M.D. Carter, and R.H. Goulding, Thin Solid Films **506**, 579 (2006).

[30] F.F. Chen, Phys. Plasmas **3**, 1783 (1997).

[31] A.W. Trivelpiece and R.W. Gould, J. Appl. Phys. **30**, 1784 (1959).

[32] F.F. Chen, *Introduction to Plasma Physics and Controlled Fusion*, 2nd ed., Vol. 1: "Plasma Physics" (Plenum Press, New York, 1984), p. 106.

[33] R.W. Boswell, J. Plasma Phys. **31**, 197 (1984).

[34] K.P. Shamrai and V.B. Taranov, Plasma Sources Sci. Technol. **5**, 474 (1996).

[35] G.G. Borg and R.W. Boswell, Phys. Plasmas **5**, 564 (1998).

[36] F.F. Chen and D. Arnush, Phys. Plasmas **4**, 3411 (1997).

[37] D.D. Blackwell, T.G. Madziwa, D. Arnush, and F.F. Chen, Phys. Rev. Lett. **88**, 145002 (2002).

[38] T. Watari, T. Hatori, R. Kumazawa, S. Hidekuma, T. Aoki, T. Kawamoto, M. Inutake, S. Hiroe, A. Nishizawa, K. Adati, T. Sato, T. Watanabe, H. Obayashi,, and K. Takayama, Phys. Fluids **21**, 2076 (1978).

[39] F.F. Chen, *Double Helix: The Dawson Separation Process*, in "From Fusion to Light Surfing", ed. by T. Katsouleas (Addison-Wesley, New York, 1991), Chap. 14.

[40] F.F. Chen, *Radiofrequency field enhancement near ion gyroresonance,* TRW Report Task II-3552 (1981), available at http://www.ee.ucla.edu/~ffchen/Archive/Chen095.pdf.

[41] D.G. Miljak and F.F. Chen, Plasma Sources Sci. Technol. **7**, 61 (1998).

[42] F.F. Chen, *Helicon Plasma Sources*, in "High Density Plasma Sources", ed. by Oleg A. Popov (Noyes Publications, Park Ridge, NJ, 1995), p. 60.

[43] P. K. Loewenhardt, B. D. Blackwell, R. W. Boswell, G. D. Conway, and S. M. Hamberger, Phys. Rev. Lett. **67**, 2792 (1991).

[44] P. Zhu and R.W. Boswell, Physics of Fluids B **3**, 869 (1991).

[45] A. R. Ellingboe, R. W. Boswell, J. P. Booth, and N. Sadeghi, Phys. Plasmas **2**, 1807 (1995).

[46] A. W. Molvik, A. R. Ellingboe, and T. D. Rognlien, Phys. Rev. Lett. **79**, 233 (1997).

[47] F.F. Chen and D.D. Blackwell, Phys. Rev. Lett. **82**, 2677 (1999).

[48] S. Cho, Phys. Plasmas **3**, 4268 (1996).

[49] I.V. Kamenski and G.G. Borg, Computer Phys. Comm. **113**, 10 (1998).

[50] D. Curreli and F.F. Chen, Phys. Plasmas **18**, 113501 (2011).

[51] X.M. Guo, J. Scharer, Y. Mouzouris, and L. Louis, Phys. Plasmas **6**, 3400 (1999).

[52] http://www.seas.ucla.edu/ltptl/presentations.htm (HELIC 10zip.exe).

[53] T.H. Stix, *Waves in Plasmas* (Springer, New York, 1992).

[54] D. Arnush and F.F. Chen, Phys. Plasmas **5**, 1239 (1998).

[55] K. P. Shamrai, Plasma Sources Sci. Technol. **7**, 499 (1998).

[56] S. Cho, Phys. Lett. A **216**, 137 (1996).

[57] S. Cho, Phys. Plasmas **3**, 4268 (1996).

[58] S. Cho and J.G. Kwak, Phys. Plasmas **4**, 4167 (1997).

[59] S.Cho and M.A. Lieberman, Phys. Plasmas 10, 882 (2003).

[60] F.F. Chen, J. Vac. Sci. Technol. A **10**, 1389 (1992).

[61] F.F. Chen, Phys. Plasmas **10**, 2586 (2003).

[62] A.W. Degeling, C.O. Jung, R.W. Boswell, and A.R. Ellingboe, Phys. Plasmas **3**, 2788 (1996).

[63] G. Sato, W. Oohara, and R. Hatakeyama, Plasma Sources Sci. Technol. **16**, 734 (2007).

[64] S. Cho, Phys. Plasmas **13**, 033504 (2006).

[65] P. Zhu and R.W. Boswell, J. Appl. Phys. **68**, 1981 (1990).

[66] A.W. Degeling and R.W. Boswell, Phys. Plasmas **4**, 2748 (1997).

[67] K. Chi, T.E. Sheridan, and R.W. Boswell, Plasma Sources Sci. Technol. **8**, 421 (1999).

[68] A.R. Ellingboe and R.W. Boswell, Phys. Plasmas **3**, 2797 (1996).

[69] F.F. Chen and H. Torreblanca, Plasma Sources Sci. Technol. **16**, 593 (2007).

[70]G. Chevalier and F.F. Chen, J. Vac. Sci. Technol. A **1**1, 1165 (1993).

[71] D.D. Blackwell and F.F. Chen, Plasma Sources Sci. Technol. **6**, 569 (1997).

[72] M. Light and F.F. Chen, Phys. Plasmas **2**, 1084 (1995).

[73] M. Light, I.D. Sudit, F.F. Chen, and D. Arnush, Phys. Plasmas **2**, 4094 (1995).

[74] S. Shinohara and T. Tanikawa, Rev. Sci. Instrum. **75**, 1941 (2004).

[75] S. Shinohara and T. Tanikawa, Phys. Plasmas **12**, 044502 (2005).

[76] T. Motomura, S. Shinohara, T. Tanikawa, and K. P. Shamrai, Phys. Plasmas **19**, 043504 (2012).

[77] S. Shinohara and T. Soejima, Plasma Phys. Control. Fusion **40**, 2081 (1998).

[78] S. Shinohara, N. Kaneda, and Y. Kawai, Thin Solid Films **316**, 139 (1998).

[79] S. Shinohara, S. Takechi, N. Kaneda, and Y. Kawai, Plasma Phys. Control. Fusion **39**, 1479 (1997).

[80] S. Shinohara and K. P. Shamrai, Plasma Phys. Control. Fusion **42**, 865 (2000).

[81] D. Kuwahara, A. Mishio, T. Nakagawa, and S. Shinohara, Rev. Sci. Instrum. 84, 103502 (2013).

[82] S. Shinohara, H. Tsuji, T. Yoshinaka, and Y. Kawai, Surface and Coatings Technology **112**, 20, (1999).

[83] S. Shinohara, N. Matsuoka, and T. Yoshinaka, Jpn. J. Appl. Phys. **38**, 4321 (1999).

[84] S. Shinohara, N. Matsuoka, and S. Matsuyama, Phys. Plasmas **8**, 1154 (2001).

[85] http://ulysses.phys.wvu.edu/ESCIME/miniconference/2007postersession.html, E.E. Scime, A.M. Keesee, and R.W. Boswell, Phys. Plasmas **15**, 058301 (2008).

[86] M. M. Balkey, R. Boivin, J. L. Kline, and E.E. Scime, Plasma Sources Sci. Technol. **10**, 284 (2001).

[87] J.L Kline, E.E. Scime, R.F. Boivin, A.M. Keesee, and X. Sun, Phys. Rev. Lett. **88**, 195002 (2002).

[88] J.L. Kline and E.E. Scime, Phys. Plasmas 10, 135 (2003).

[89] M. Krämer, Yu. M. Aliev, A. B. Altukhov, A.D. Gurchenko, E.Z. Gusakov, and K. Niemi, Plasma Phys. Control. Fusion **49**, A167 (2007).

[90] B. Lorenz, M. Krämer, V.L. Selenin, and Yu.M. Aliev, Plasma Sources Sci.Technol. **14**, 623 (2005).

[91] B. Fischer, M. Krämer, and Th. Enk, Plasma Phys. Control. Fusion **36**, 2003 (1994).

[92] Y. Sakawa, T. Takino, and T. Shoji, Appl. Phys. Lett. **73**, 1643 (1998).

[93] Y. Sakawa, N. Koshikawa, and T. Shoji, Plasma Sources SCi. Technol. **6**, 96 (1997).

[94] Y. Sakawa, T. Takino, and T. Shoji, Phys. Plasmas **6**, 4759 (1999).

[95] Y. Mori, H. Nakashima, F.W. Baity, R.H. Goulding, M.D. Carter, and D.O. Sparks, Plasma Sources Sci. Technol. **13**, 424 (2004).

[96] S.M. Yun, J.H. Kim, and H.Y. Chang, J. Vac. Sci. Technol. A **15**, 3 (1997).

[97] J.H. Kim, S.M. Yun, and H.Y. Chang, IEEE Trans. Plasma Sci. **24**, 1364 (1996).

[98] S.M. Yun, J.H. Kim, and H.Y. Chang, IEEE Trans. Plasma Sci. 26, 159 (1998)

[99] S.M. Yun, S. Cho, G. Tynan, and H.Y. Chang, Phys. Plasmas **8**, 358 (2001).

[100] J.H. Kim and H.Y Chang, Phys. Plasmas **3**, 1462 (1996).

[101] G.S. Eom, I.D. Bae, G. Cho, Y.S. Hwang, and W. Choe Plasma Sources Sci. Technol. **10**, 417 (2001).

[102] G.S. Eom and W. Choe, J. Vac. Sci. Technol. A **20**, 2079 (2002).

[103] G.S. Eom, J. Kim, and W. Choe, Phys. Plasmas **13**, 73505 (2006).

[104] P.K. Loewenhardt, B.D. Blackwell, and S.M. Hamberger, Plasma Phys. Control. Fusion **37**, 229 (1995).

[105] B.C. Zhang, G.G. Borg, and B.D. Blackwell, Plasma Phys. **2**, 803 (1995).

[106] L. Chang, M.J. Hole, J.F. Caneses, G. Chen, B.D. Blackwell, and C.S. Corr, Phys. Plasmas **19**, 083511 (2012).

[107] C.M. Franck, O. Grulke, A. Stark, T. Klinger, E.E. Scime, and G. Bonhomme, Plasma Sources Sci. Technol. **14**, 226 (2005).

[108] C.S. Corr, N. Plihon, P. Chabert, O. Sutherland, and R.W. Boswell, Phys. Plasmas **11**, 4596 (2004).

[109] C. S. Corr, N. Plihon, and P. Chabert, J. Appl. Phys. **99**, 103302 (2006).

[110] R. Petri, N. Sadeghi, and D. Henry, J. Vac. Sci. Technol. A **13**, 2930 (1996).

[111] B.B. Sahu and A. Dangi, Dronacharya Research Journal **3**, 89 (2011).

[112] B.B. Sahu, Dronacharya Research Journal **4**, 17 (2012).

[113] A. Ganguli, B.B. Sahu, and R.D. Tarey, Phys. Plasmas **14**, 113503 (2007).

[114] A. Ganguli, B.B. Sahu, and R.D. Tarey, Phys. Plasmas **20**, 013510 (2013).

[115] M.K. Paul and D. Bora, Phys. Plasmas **14**, 082507 (2007).

[116] V.P. Anitha, D. Sharma, S.P. Banerjee, and S.K. Mattoo, Phys. Plasmas **19**, 082118 (2012).

[117] R.D. Tarey, B.B. Sahu, and A. Ganguli, Phys. Plasmas **19**, 073520 (2012).

[118] K.K. Barada, P.K. Chattopadhyay, J. Ghosh, S. Kumar, and Y.C. Saxena, Phys. Plasmas **20**, 012123 (2013).

[119] J. Gilland, R. Breun, and N. Hershkowitz, Plasma Sources Sci. Technol. 7, 418 (1998).

[120] R.T.S. Chen and N. Hershkowitz, Phys. Rev. Lett. **80**, 4677 (1998).

[121] X.M. Guo, J. Scharer, Y. Mouzouris, and L. Louis, Phys. Plasmas **6**, 3400 (1999).

[122] Y. Mouzouris and J. E. Scharer, IEEE Trans. Plasma Sci. **27**, 66 (1999).

[123] M.P. Reilly and G.H. Miley, Plasma Sources Sci. Technol. **19**, 045006 (2010).

[124] G.R. Tynan, M.J. Burin, C. Holland, G. Antar, and N. Crocker, Phys. Plasmas **11**, 5195 (2004).

[125] P. H. Diamond and Y.-B. Kim, Phys. Fluids B **3**, 1626 (1991).

[126] C. Holland, J.H. Yu, A. James, D. Nishijima, M Shimada, N. Tahori, and G. R. Tynan, Phys. Rev. Lett. **96**, 195002 (2006).

[127] S. C. Thakur, D. McCarren, T. Lee, N. Fedorczak, P. Manz, E.E. Scime, G.R. Tynan, and M. Xu, Phys. Plasmas **19**, 082102 (2012).

[128] B.N. Breizman and A. V. Arefiev, Phys. Rev. Lett. **84**, 3863 (2000).

[129] B.N. Breizman and A. V. Arefiev, Phys. Plasmas **9**, 1015 (2002).

[130] L. Porte, S.M. Yun, F.F. Chen, and D. Arnush, Plasma Sources Sci. Technol. **12**, 287 (2003).

[70] M. Light, F.F. Chen, and P.L. Colestock, Plasma Sources Sci. Technol. **11**, 273 (2002).

[132] G.R. Tynan, M.J. Burin, C. Holland, G. Antar, and P.H. Diamond, Plasma Phys. Control. Fusion **46**, A373 (2004).

[133] F.F. Chen, Phys. Plasmas **19**, 093509 (2012).

[134] S. Shinohara and T. Tanikawa, Rev. Sci. Instrum. **75**, 1941 (2004).

[135] S. Shinohara and T. Tanikawa, Phys. Plasmas **12**, 44502 (2005).

[136] T. Motomura, S. Shinohara, T. Tanikawa and K. P. Shamrai, Phys. Plasmas **19**, 043504 (2012).

[137] Matsushita, J., Sasaki, K., and Kadota, K., Jpn. J. Appl Phys. 1 **36**, 4747 (1997).

[138] S. Shinohara, H. Tsuji, T. Yoshinaka, and Y. Kawai, Surface Coatings and Technol. **112**, 20 (1999).

[139] R.T.S. Chen, R.A. Breun, S. Gross, N. Hershkowitz, M.J. Hsieh, and J. Jacobs, Plasma Sources Sci. Technol.**4**, 337 (1995).

[140] A. G. Lynn, M. Gilmore, C. Watts, J. Herrea, R. Kelly, S. Xie, L. Yan and Y. Zhang, Rev. Sci. Instrum. **80**, 103501 (2009).

[141] F.R. Chang-Diaz, Thin Solid Films **506–507**, 449 (2006).

[142] R. W. Boswell, O. Sutherland, C. Charles, J.P. Squire, F.R. Chang-Diaz, T.W. Glover, V.T. Jacobson, D.G. Chavers, R.D. Bengtson, E.A. Bering III, R.H. Goulding, and M. Light, Phys. Plasmas **11**, 5125 (2004).

[143] J.P. Squire, F. R. Chang-Diaz, T.W. Glover, V.T. Jacobson, G.E. McCaskill, D.S. Winter, F.W. Baity, M.D. Carter, and R.H. Goulding, Thin Solid Films **506**, 579 (2006).

[144] R. Winglee, T. Ziemba, L. Giersch L. J. Prager, J. Carscadden, and B. R. Roberson, Phys. Plasmas **14**, 063501 (2007).

[145] J. Prager, R. Winglee, T. Ziemba, and B. R. Roberson, Plasma Sources Sci. Technol. **17**, 025003 (2008).

[146] F.F. Chen, IEEE Trans. Plasma Sci. (submitted, 2014).

[147] K.P. Shamrai, V.P. Pavlenko, and V.B. Taranov, Plasma Phys. Control. Fusion **39**, 505 (1997).

[148] C. Carter and J. Khachan, Plasma Sources Sci. Technol. **8**, 432 (1999).

[149] C. Charles, J. Vac. Sci. Technol. A **11**, 157 (1993).

[150] wikipedia.org

[151] P.K. Loewenhardt, B.D. Blackwell, R.W. Boswell, G.D. Conway, and S.M. Hamberger, Phys. Rev. Lett. **67**, 2792 (1991).

[152] Y. Sakawa, M. Ohshima, Y. Ohta, and T. Shoji, Phys. Plasmas **11**, 311 (2004).

[153] N. Benjamin, B. Chapman, and R. Boswell, Proceedings of SPIE **1392**, 95 (1991).

[154] I. Tepermeister, N. Blayo, F.P. Klemens, D.E. Ibbotson, R.A. Gottscho, and J.T.C. Lee, J. Vac. Sci. Technol. B **12**, 2310 (1994).

[155] I Tepermeister, D.E. Ibbotson, J.T.C. Lee, and H.H. Sawin, J. Vac. Sci. Technol. B **12**, 2322 (1994).

[156] G.W. Gibson, Jr., H.H. Sawin, I. Tepermeister, D.E. Ibbotson, and J.T.C. Lee, J. Vac. Sci. Technol. B **12**, 2333 (1994).

[157] G.R. Tynan, A.D. Bailey III, G.A. Campbell, R. Charatan, A. de Chambrier, G. Gibson, D.J. Hemker, K. Jones, A. Kuthi, C. Lee, T. Shoji, and M. Wilcoxson, J. Vac. Sci. Technol. A **15**, 2885 (1997).

[158] F.F. Chen, J.D. Evans, and G.R. Tynan, Plasma Sources Sci. Technol. **10**, 236 (2001).

[159] F.F. Chen, X. Jiang, and J.D. Evans, J. Vac. Sci. Technol. A **18**, 2108 (2000).

[160] M. Yano and M.L.R. Walker, Phys. Plasmas **13**, 063501 (2006) and **14**, 033510 (2007).

[161] F.F. Chen, *Helicon source for ion propulsion*, Encyclopedia of Plasma Technology (Taylor and Francis, New York, to be published, 2014).

[162] F.F. Chen, *Introduction to Plasma Physics and Controlled Fusion*, 2nd ed., Vol. 1: "Plasma Physics" (Plenum Press, New York, 1984), p. 293.

[163] C. Charles, Plasma Sources Sci. Technol. **16**, R1 (2007).

[164] F.F. Chen, Phys. Plasmas **13**, 034502 (2006).

[165] E.B. Hooper, J. Propulsion Power **9**, 757 (1993).

[166] Winglee, R., Ziemba,T., Giersch, L., Prager, J., Carscadden, J., and Roberson, B.R. Phys. Plasmas **14**, 063501 (2007).

[167] N. Singh, S. Rao, and P. Ranganath, Phys. Plasmas **20**, 032111 (2013).

[168] M. Merino and E. Ahedo, Plasma Sources Sci. Technol. **23**,032001 (2014).

[169] K.M. Lemmer, A.D. Gallimore, and T.B. Smith, Plasma Sources Sci. Technol. **18**, 025019 (2009).

[170] K. Takahashi, T. Lafleur, C. Charles, P. Alexander, R.W. Boswell, M. Perren, R. Laine, S. Pottenter, V. Lappas, T. Harle, and D. Lamprou, Appl. Phys. Lett. **98,** 141503 (2011).

[171] F.F. Chen, Phys. Plasmas **19**, 093509 (2012).

[172] F.F. Chen and D. Curreli, Phys. Plasmas **20**, 057102 (2013)

[173] F.F. Chen and H. Torreblanca, Plasma Phys. Control. Fusion **49**, A81 (2007).

[174] F.F. Chen and H. Torreblanca, Phys. Plasmas **16**, 057102 (2009).